The ER membrane protein complex is required to ensure correct topology and stable expression of flavivirus polyproteins

Ashley M Ngo[1], Matthew J Shurtleff[2], Katerina D Popova[2], Jessie Kulsuptrakul[1], Jonathan S Weissman[2,3], Andreas S Puschnik[1,4]

[1] Chan Zuckerberg Biohub, San Francisco, United States

[2] Department of Cellular and Molecular Pharmacology, University of California, San Francisco, United States

[3] Howard Hughes Medical Institute, University of California, San Francisco, United States

[4] Correspondence: andreas.puschnik@czbiohub.org

Abstract

Flaviviruses translate their genomes as multi-pass transmembrane proteins at the endoplasmic reticulum (ER) membrane. Here, we show that the ER membrane protein complex (EMC) is indispensable for the expression of viral polyproteins. We demonstrated that EMC was essential for accurate folding and post-translational stability rather than translation efficiency. Specifically, we revealed degradation of NS4A-NS4B, a region rich in transmembrane domains, in absence of EMC. Orthogonally, by serial passaging of virus on EMC-deficient cells, we identified two non-synonymous point mutations in NS4A and NS4B, which rescued viral replication. Finally, we showed a physical interaction between EMC and viral NS4B and that the NS4A-4B region adopts an aberrant topology in the absence of the EMC leading to degradation. Together, our data highlight how flaviviruses hijack the EMC for transmembrane protein biogenesis to achieve optimal expression of their polyproteins, which reinforces a role for the EMC in stabilizing challenging transmembrane proteins during synthesis.

24 **Introduction**

25 Flaviviruses such as dengue (DENV), Zika (ZIKV) or West Nile virus (WNV) express their genome
26 as a single multi-pass transmembrane protein at the endoplasmic reticulum (ER) membrane.
27 Subsequently, the polyprotein is cleaved by the viral NS2B-NS3 protease and the cellular signal
28 peptidase into the individual structural (C, prM, E) and non-structural (NS1-5) proteins required
29 for replication and assembly into new virions (Neufeldt et al., 2018). Similar to cellular
30 transmembrane proteins, the viral polyprotein relies on the host cell machinery for targeting to the
31 ER, translocation across the membrane and insertion of transmembrane domains (TMDs) into
32 the lipid bilayer during its translation. These processes are facilitated by the signal recognition
33 particle (SRP), the translocon-associated protein (TRAP) complex (also known as signal-
34 sequence receptor complex), the Sec61 translocon and the signal peptidase complex. These cell
35 components were all identified as essential host factors for flavivirus infection in genetic screens
36 underscoring their importance for virus replication (Krishnan et al., 2008; Marceau et al., 2016;
37 Sessions et al., 2009; Zhang et al., 2016). For most transmembrane proteins, recognition of a
38 hydrophobic TMD or signal sequence by the SRP followed by transfer to the Sec61 translocation
39 channel are sufficient for membrane targeting and accurate topogenesis (Shao and Hegde, 2011).
40 Recently, it was shown that the ER membrane protein complex (EMC) plays a role in the insertion
41 and/or stabilization of certain transmembrane proteins (Chitwood et al., 2018; Guna et al., 2018;
42 Shurtleff et al., 2018). Intriguingly, several genome-wide CRISPR knockout (KO) screens for
43 flavivirus dependency factors showed strong enrichment of the EMC (Ma et al., 2015; Marceau
44 et al., 2016; Savidis et al., 2016; Zhang et al., 2016). However, its role in the virus life cycle is not
45 yet understood.

46 The EMC was originally discovered in a genetic screen for yeast mutants modulating the unfolded
47 protein response (UPR) (Jonikas et al., 2009). Genetic interaction mapping and biochemical
48 purification revealed a six-subunit core complex (EMC1-6) conserved in yeast and mammals
49 (Christianson et al., 2011; Jonikas et al., 2009). Other than its more general association with UPR

50 and ER-associated degradation (ERAD), the EMC was shown to interact co-translationally and
51 enable biogenesis of a subset of multi-pass transmembrane proteins (Shurtleff et al., 2018).
52 Biochemical characterization of select EMC client proteins, such as tail-anchored proteins and G
53 protein-coupled receptors (GPCRs), revealed that the EMC is capable of inserting TMDs into the
54 ER membrane (Chitwood et al., 2018; Guna et al., 2018). Here, we investigated how the
55 mosquito-borne flaviviruses, such as DENV, ZIKV and WNV, depend on the EMC for their
56 polyprotein biogenesis during infection.
57
58 **Results**
59 To validate the enrichment of EMC components in the flavivirus CRISPR screens, we generated
60 isogenic EMC subunit KO cell lines in Huh7.5.1 and HEK293FT, two cell types that were used for
61 the genetic screens (Figure 1 - figure supplement 1A). Upon infection with DENV expressing
62 Renilla luciferase (DENV-Luc), we measured a ~10,000-fold reduction in viral replication in
63 Huh7.5.1 EMC1-6 KO cells (Figure 1A) and a 10-1,000-fold reduction in HEK293FT EMC1-5 KO
64 cells (Figure 1B). The differences in the extent of the phenotypes may be attributed to the
65 presence of compensatory pathways or the degree of disruption of the entire protein complex
66 between the two cell types upon knockout of a single subunit. The strong deficit in DENV
67 replication in the absence of the EMC persisted over a 30-72h period (Figure 1 - figure supplement
68 1B). Complementation of EMC2 and EMC4 KO cells with the respective cDNA completely
69 restored levels of DENV infection (Figure 1C and Figure 1 - figure supplement 1C). Lastly, we
70 tested the effect of EMC4 KO on several flaviviruses and saw a significant decrease of viral RNA
71 for DENV, WNV and ZIKV but not hepatitis C virus (HCV), which is a more distantly related
72 member of the *Flaviviridae* family (Figure 1D and Figure 1 - figure supplement 1D). This is
73 congruent with results of an HCV CRISPR screen that did not identify the EMC as a critical host
74 factor (Marceau et al., 2016). This finding highlights that there is a specific, evolutionarily
75 conserved dependency on the EMC among mosquito-borne flaviviruses and not a universal

76 disruption of trafficking to and/or translation or replication at the ER membrane, which would affect
77 a wider range of viruses.
78
79 Next, we sought to determine at which step of the viral life cycle the EMC is required. As the EMC
80 is important for the expression of a large set of transmembrane proteins, its disruption leads to an
81 altered cell surface proteome, which may affect viral attachment to cells and/or entry. We
82 measured effects on viral binding and uptake by quantifying the amount of viral RNA after virus
83 incubation with WT and EMC4 KO cells at 2 and 6 hours post-infection (hpi), where we did not
84 observe a difference (Figure 2A). Only at 24hpi, a timepoint when viral replication had occurred,
85 was a difference in RNA load evident between WT and EMC4 KO cells. Furthermore, we used a
86 DENV replicon expressing luciferase, which bypasses entry and does not produce viral particles,
87 thus allowing the analysis of the effect of EMC KO specifically on translation and replication. In
88 this assay, we saw decreased luminescence in EMC4 KO cells starting at 12 hours post-
89 electroporation suggesting that the EMC is important during or prior to viral replication (Figure
90 2B). We additionally performed the replicon assay in the presence of MK-0608, a nucleoside
91 analogue that inhibits the viral polymerase (Chen et al., 2015), and observed that the
92 luminescence signal in EMC4 KO cells was lower than in replication-inhibited WT cells suggesting
93 that deletion of EMC has an effect on viral translation, which happens prior to replication (Figure
94 2 - figure supplement 1A). To further dissect effects on translation or genome replication of DENV,
95 we conducted an immunoblot timecourse series, where WT and EMC4 KO cells were infected at
96 a high multiplicity of infection (moi=32) and lysates were harvested at early timepoints post-
97 infection (6-12hpi), when no or only little DENV replication had occurred. Viral protein expression
98 was lower in EMC4 KO compared to WT cells as early as 6hpi further supporting a translation
99 defect (Figure 2C). To rule out any contribution of low levels of replication to the observed
100 phenotype, we also performed the immunoblot experiment in the presence of MK-0608 and still
101 saw different amounts of DENV protein accumulation between WT and EMC4 KO cells indicating

102 that the EMC is indeed important for viral protein expression (Figure 2 - figure supplement 1B).
103 Interestingly, while the EMC has been implicated in the stable biogenesis of transmembrane
104 proteins, we found reduced expression of both TMD and non-TMD containing viral proteins. This
105 suggests that the defect likely occurs at the polyprotein stage thus affecting all individual, cleaved
106 proteins.
107
108 The expression of flaviviral proteins is a complex process that requires several steps. DENV
109 translation is initiated in a cap-dependent manner, whereupon the single-stranded positive-sense
110 RNA genome is translated into a single ~3,400 amino acid long multi-pass transmembrane
111 protein. This polyprotein is co- and post-translationally processed by host and viral proteases
112 producing the individual structural and non-structural proteins. We first tested whether the defect
113 occurs at the stage of polyprotein translation. We used ribosome profiling (Ribo-seq), which
114 measures the density of ribosomes on a given mRNA species with high positional resolution, to
115 compare translation efficiencies (TE) and successful full-length synthesis of both cellular and viral
116 proteins in WT and EMC4 KO cells (Ingolia et al., 2009). Any changes in TE or premature
117 ribosome stalling in EMC KO vs WT cells would be reflected by changes in ribosomal footprints
118 (as measured by ribosome profiling) normalized to changes in mRNA abundance (as measured
119 by RNA-seq). In the uninfected condition, we did not observe dramatic changes in TE for cellular
120 mRNAs in EMC4 KO vs WT cells (Figure 3A and Figure 3 - Source Data 1). This is in line with
121 previously reported results using CRISPRi knockdown against EMC subunits suggesting that
122 deletion of EMC minimally impacts the synthesis rates of its client proteins (Shurtleff et al., 2018).
123 Similarly, we did not find any substantial differences in viral TE in EMC4 KO cells relative to WT
124 cells at 18 (0.43x) and 44hpi (2.17x) (Figures 3B and 3C and Figure 3 - Source Data 1). Instead,
125 we observed that DENV RNA was among the highest translated (top 0.1%) mRNAs in both WT
126 and EMC4 KO cells (Figure 3 - figure supplement 1A). The lower number of ribosomal footprints
127 aligning to the viral genome in EMC4 KO cells was largely due to the reduced number of viral

128 RNA copies present in the cells. Moreover, footprints were found to map throughout the viral
129 genome in EMC4 KO cells, indicating that synthesis of full-length polyprotein still occurred (Figure
130 3 - figure supplement 1B). Therefore, we concluded that translation of DENV polyproteins is not
131 strongly impacted by loss of EMC, which led us to explore potential post-translational defects.
132 Proper insertion of TMDs and correct folding are required for stable expression of transmembrane
133 proteins, while misfolded proteins are generally targeted to the proteasome for degradation via
134 the ERAD pathway (Olzmann et al., 2013). To probe whether an increased fraction of viral
135 proteins is degraded by the proteasome in EMC deficient cells, we infected WT and EMC4 KO
136 cells with DENV in the presence of Bortezomib (BZ), a proteasome inhibitor, thus preventing
137 removal of misfolded proteins from the cells. Indeed, BZ treatment led to an increase of detectable
138 viral proteins in EMC4 KO cells but not WT cells (Figure 3D). Addition of BZ, however, did not
139 restore DENV replication arguing that the proteasome-targeted proteins are non-functional
140 (Figure 3 - figure supplement 2). Together, this suggests that in the absence of EMC viral proteins
141 are still translated but are unable to achieve a stable conformation resulting in their degradation
142 and inability to establish efficient replication.
143
144 For cellular multi-pass client proteins, such as transporters and GPCRs, the EMC co-
145 translationally engages with specific TMDs in order to support insertion into the membrane and
146 allow stable expression of the entire transmembrane protein (Chitwood et al., 2018; Shurtleff et
147 al., 2018). We used two orthogonal methods, a fluorescence-based protein stability assay and
148 viral evolution, to examine which region of the viral polyprotein requires the EMC for successful
149 expression. First, we utilized a dual-color fluorescent reporter as previously described (Chitwood
150 et al., 2018). The C terminus of different segments of the DENV polyprotein was fused to eGFP
151 followed by a viral T2A sequence and mCherry (G2C) (Figure 4A). Translation of the fusion
152 constructs generates two protein products at a 1:1 ratio due to peptide bond skipping by the
153 ribosome at the T2A site: 1) a polyprotein segment fused to eGFP and 2) mCherry. Any post-

154 translational instability of the eGFP fusion protein due to misfolding results in an eGFP:mCherry
155 ratio of less than 1. As expected, the cytosolic G2C-only construct displayed a 1:1 ratio in both
156 WT and EMC4 KO cells, while the β_1-adrenergic receptor (ADRB1) fused to G2C exhibited drastic
157 destabilization in EMC4 KO compared to WT cells as was previously reported (Figure 4B)
158 (Chitwood et al., 2018). Applying this approach to different DENV polyprotein G2C fusion
159 constructs, we observed that the segments containing only the structural proteins (capsid, prM
160 and E) or NS1-3 were not destabilized in EMC4 KO Huh7.5.1 cells (Figure 4B). By contrast,
161 constructs encoding both NS4A and NS4B (but not either of them alone) showed reduced stability
162 in EMC4 KO cells (Figure 4B). Similar results were obtained in HEK293FT (Figure 4 - figure
163 supplement 1). NS4A has 3 TMDs with the third (termed 2K peptide) being highly hydrophobic
164 and serving as a signal sequence for the translocation of NS4B into the ER membrane (Lin et al.,
165 1993). Subsequently, the NS4A-2K junction is cleaved by the viral protease and the 2K-NS4B
166 junction by the signal peptidase. As the 2K-targeted NS4B-5-G2C construct did not display a
167 stability defect in EMC deficient cells, the results suggest that EMC mediates stable expression
168 by first engaging within NS4A prior to the 2K peptide and that a defect in NS4A is extended to the
169 NS4B region. Stability of NS4A-4B-G2C was restored to near WT levels by complementation of
170 EMC4 KO cells with EMC4 cDNA (Figure 4C). Moreover, treatment of EMC4 KO cells with BZ
171 increased the eGFP:mCherry ratio of NS4A-4B-G2C in EMC4 KO cells indicating that this region
172 of the polyprotein is misfolded and targeted for degradation in the absence of EMC (Figure 4D).
173 Therefore, we linked the DENV replication phenotype in EMC deficient cells to a specific
174 molecular defect in the NS4A-4B region of the polyprotein.
175
176 In a second, orthogonal approach, we performed viral adaptation to evolve EMC-independent
177 DENV mutants by passaging the virus consecutively on EMC4 KO Huh7.5.1 cells every 3-4 days.
178 After 20-22 passages we observed cell death in 3 out of 6 independent adaptation experiments.
179 Sequencing of RNA extracted from supernatant and alignment to the WT16681 DENV genome

180 revealed two non-synonymous point mutations in NS4A and NS4B, which were conserved across
181 all three isolates (Figure 5A). The A6665G mutation led to a tyrosine to cysteine and the A7558T
182 mutation to an asparagine to tyrosine substitution. The majority of other SNPs was silent (Figure
183 5 - figure supplement 1). A6665G is predicted to be inside a TMD helix encoding region of NS4A
184 suggesting that this TMD relies on the EMC for proper ER membrane insertion (Miller et al., 2007).
185 Only one of 1,359 DENV serotype 2 genomes from the NCBI database has a G at this position
186 encoding cysteine, while other sequences all encode tyrosine. This evolutionary conservation
187 suggests that this residue indeed has an important function. Similarly, the frequency of A at
188 position 7558 is very conserved with 99.6%, and there is no T encoding tyrosine in the 1,359
189 sequenced strains. Interestingly, A7558T resides in a non-TMD region at the end of NS4B, thus
190 likely not supporting membrane insertion but folding in a different manner (Miller et al., 2006). For
191 all three EMC adapted isolates, replication levels in EMC4 KO cells were similar to levels in WT
192 cells, while WT16681 DENV displayed a ~100-fold reduction in viral RNA in EMC4 KO relative to
193 WT cells (Figure 5 - figure supplement 2A). The same effect was observed in a 72h viral growth
194 curve (Figure 5B). The adapted virus appeared less fit than the WT DENV at earlier timepoints
195 but reached similar levels of replication at 72 hpi suggesting that the adaptive mutations did not
196 cause dramatic growth defects.
197 To dissect whether both mutations are required for optimal replication in EMC KO background,
198 we introduced them individually or in tandem into the DENV-Luc infectious clone and generated
199 virus. While A6665G and A7558T individually restored DENV replication in EMC4 KO cells to 30
200 and 86% of WT levels, respectively, the double mutant displayed complete rescue of viral growth
201 in EMC KO cells (Figure 5C). Similarly, we measured ~10- and 100-fold higher replication levels
202 for the single and double mutant DENV-Luc, respectively, compared to WT DENV-Luc in EMC
203 KO cells over a 72h period, while replication in WT cells was comparable (Figure 5 - figure
204 supplement 2B). We also introduced the two adaptive mutations into NS4A-5-G2C, which showed
205 increased stability in EMC4 KO cells compared to the WT construct thus reverting the molecular

206 destabilization phenotype (Figure 5D). Remarkably, the G2C fluorescence assay and viral
207 adaptation independently pinpointed NS4A-4B of the polyprotein as the region, which requires
208 the EMC. The results of the two experiments suggest that a defect in the stable insertion of the
209 NS4A TMD2 could lead to an aberrant topology / instability of NS4B. By contrast, polyprotein
210 segments starting with 2K-NS4B were stably expressed in EMC KO cells as was shown using
211 NS4B-5-G2C construct (Figure 4A). Therefore, the EMC is required for correct insertion,
212 processing and/or folding of the NS4A-4B region.
213
214 To probe further how absence of EMC causes failure of DENV replication, we transfected a
215 subgenomic NS2B-4B construct (containing functional NS2B-NS3 for polyprotein cleavage) with
216 a C-terminal fusion to eGFP into WT and EMC4 KO cells and immunoblotted against the different
217 processed products. While there was no notable difference in expression levels between the
218 higher molecular weight intermediates (NS2B-NS3-NS4A-NS4B-eGFP or NS4A-NS4B-eGFP),
219 we observed reduced accumulation of processed NS4B-eGFP in EMC4 KO cells (Figure 6A). BZ
220 treatment indicated rapid degradation of cleaved NS4B-eGFP in EMC deficient cells.
221 Furthermore, if the EMC acts to insert or stabilize NS4A-4B, we hypothesized that direct binding
222 of NS4B to EMC post polyprotein-processing should be detectable in WT cells. We performed a
223 co-immunoprecipitation using FLAG-tagged EMC4 and detected NS4B but not prM or NS5 in the
224 pulldown (Figure 6B). This supports the finding that EMC physically engages with NS4A-4B to
225 facilitate its biogenesis and stable expression. Interestingly, we also detected physical interaction
226 between the EMC and NS4B of the adapted DENV (Figure 6C). This suggests that the two amino
227 acid substitutions in the NS4A and NS4B viral proteins do not ablate the signal triggering EMC
228 engagement. The mutations may rather allow the virus to maintain proper folding and stability in
229 the absence of the EMC.
230 Finally, we examined the topology of the NS4A-4B transmembrane protein region in WT and EMC
231 deficient cells using a protease protection assay. We generated different constructs, in which

232 eGFP was C-terminally fused after different TMDs that had been determined experimentally
233 (Figure 6D) (Miller et al., 2006). Transfected cells were left untreated or treated with digitonin and
234 proteinase K followed by immunoblot. In the case of luminal localization, eGFP is protected
235 against protease digestion, while cytoplasmic eGFP is degraded. Our results showed that in WT
236 cells eGFP fused after NS4B TMD1 and TMD4 is luminal, which is consistent with the previously
237 determined topology of NS4B (Figure 6D) (Miller et al., 2006). By contrast, we did not observe
238 luminal localization for NS4B TMD1 and TMD4 in EMC4 KO cells, which indicates that EMC is
239 required for the achieving the correct topology and thus stable expression of NS4B. We
240 additionally probed the topology of NS4A using a deglycosylation assay similar to a previous study
241 (Miller et al., 2007). We introduced an opsin tag containing a glycan acceptor site downstream of
242 NS4A TMD2, which had been determined to be in the ER lumen and should therefore be
243 glycosylated. We observed efficient glycosylation in WT cells (as expected) but very poor
244 glycosylation in EMC4 KO cells, indicating an aberrant topology (Figure 6E). Moreover, we sought
245 to test whether the adaptive mutations restore the topology of NS4A-4B or allow the virus to
246 replicate with a different topology in the absence of the EMC. Since a topological defect was
247 observed early in NS4A-4B and membrane translocation occurs co-translationally, we focused on
248 the A6665G mutation, which is located in TMD2 of NS4A, rather than the A7558T mutation near
249 the C-terminus of NS4B. As the A6665G mutation led to a significant increase in replication in
250 EMC deficient cells, we would expect any rescue of correct topology to be visible. However, no
251 increase of glycosylation was observed in EMC4 KO cells using the NS4A-TMD2-opsin construct
252 containing the adaptive mutation (Figure 6E). Therefore, we conclude that the adaptive mutation
253 in NS4A does not immediately restore the correct topology but instead allows the virus to replicate
254 with NS4A-4B assuming an aberrant topology. However, we cannot exclude that the adaptive
255 mutations, which were selected by passaging full virus, only restore the wild-type topology in the
256 context of full-length viral polyprotein, for example through interactions with other viral proteins.

257 **Discussion**

258 Based on our results and previous work (Chitwood and Hegde, 2019; Shurtleff et al., 2018) we
259 propose the following model for the role of the EMC in flavivirus infection. During translation of
260 the polyprotein the EMC engages with TMDs in NS4A and NS4B to ensure their accurate
261 topology, correct folding and stable expression (Figure 6F). In the absence of the EMC, TMDs in
262 the NS4A-4B region are not accurately or stably integrated in the ER membrane leading to
263 misfolding and degradation of processed NS4B (and potentially also NS4A). Based on the
264 molecular weight of the detected bands in the protease protection assay (Figure 6D), we expect
265 that cleavage between 2K and NS4B by the signal peptidase still occurs in EMC deficient cells,
266 which is consistent with previously observed processing of dengue NS4A-2K-NS4B (Cahour et
267 al., 1992). This suggests that the N-terminus of NS4B is still localized to the ER lumen (at least
268 while being translated) in EMC KO cells. However, unlike in WT cells, where the TMD1 and TMD4
269 of NS4B are luminal, their termini are localized to the cytoplasmic site of the ER membrane in
270 EMC KO cells highlighting that EMC is required for achieving the correct topology of NS4B. Our
271 data suggests that EMC does not affect ER targeting and translocation of 2K but it still remains
272 an open question whether EMC facilitates proper insertion of TMDs into the membrane or if it is
273 required for maintaining the correct topology in a chaperone-like function post membrane
274 integration.

275 NS4A and NS4B fulfill crucial functions for viral replication. NS4A induces ER membrane
276 rearrangements important for the formation of viral replication complexes (Miller et al., 2007;
277 Roosendaal et al., 2006) while NS4B interacts with the NS3 helicase and also suppresses the
278 cellular interferon response (Muñoz-Jordán et al., 2005; Zou et al., 2015). Additionally, it was
279 demonstrated that the NS4A-2K-NS4B precursor interacts with NS1, important for viral replication
280 (Płaszczyca et al., 2019).

281 Recently, another study found that biogenesis of DENV and ZIKV NS4A and NS4B is dependent
282 on the EMC (Lin et al., 2019). While Lin et al. used ectopic expression of individual viral proteins

283 to identify NS4A and NS4B as EMC client proteins, we performed a fluorescent based stability
284 assay expressing different fragments of the viral polyprotein leading to similar conclusions.
285 However, we only observed destabilization when NS4B was preceded by NS4A arguing that the
286 NS4A-4B intermediate triggers an EMC-dependent process. Both studies showed that the EMC
287 physically interacts with NS4B to facilitate stable expression and that, in absence of EMC, NS4B
288 is misfolded and targeted for degradation as demonstrated by proteasomal inhibition. Lin et al.
289 showed that NS4B is still membrane associated in EMC deficient cells, while we provided further
290 molecular insights that NS4A-4B assumes an aberrant topology at the ER membrane.
291 Furthermore, bioinformatic prediction of NS4B transmembrane regions revealed that the two N-
292 terminal domains are only weakly hydrophobic, which could explain the dependence of NS4B on
293 the EMC for stable expression (Lin et al., 2019). This is consistent with the systematic analysis of
294 cellular EMC client proteins, which showed an underrepresentation of hydrophobic and an
295 overrepresentation of charged and aromatic amino acids within their TMDs compared to all TMDs
296 in the proteome (Shurtleff et al., 2018). Consequently, Lin et al. demonstrated that substitution of
297 all polar and charged residues inside TMD1 and TMD2 of NS4B to hydrophobic leucines led to
298 complete rescue of ectopic NS4B expression in EMC depleted cells. However, it remains unclear
299 whether these substitutions would allow for viral replication in the full polyprotein context. By
300 contrast, our EMC KO adapted mutations do not reside in TMD1 and TMD2 of NS4B but in NS4A
301 TMD2 and near the C-terminus of NS4B, and were shown to increase NS4A-4B expression levels
302 as well as restore viral replication. Overall, both studies are complimentary and in large
303 agreement, and together provide a detailed picture of how the EMC ensures stable expression of
304 two viral multi-pass transmembrane proteins.
305 Interestingly, we found that the A6665G mutation inside NS4A TMD2 does not restore the wild-
306 type topology. The A6665G mutation also arose during DENV adaptation to cell lines deficient in
307 the oligosaccharyltransferase (OST) complex, another critical host factor inside the ER membrane
308 (Marceau et al., 2016; Puschnik et al., 2017). The OST complex has been shown to be important

309 for RNA genome replication in a catalytically independent function and was suggested to act as
310 structural scaffold for viral replication complexes. It is thus possible that the tyrosine to cysteine
311 substitution generally modulates ER integration of NS4A-4B or exposes a binding interface
312 important for replication complex formation, thus likely rescuing replication without restoring the
313 normal topology. Since membrane proteins are co-translationally translocated across and
314 inserted into the membrane, it is unlikely that the A7558T mutation downstream of the apparent
315 topology defect restores proper membrane integration. Possibly, the substituting tyrosine may
316 stabilize the cytosolic orientation of the C-terminus through expansion of the "aromatic belt"
317 (Granseth et al., 2005) to allow for efficient viral protease cleavage or facilitate other critical
318 protein-protein interactions.
319 The isolation of EMC-independent DENV mutants additionally enables drug screening for EMC
320 modulators by testing compounds against WT DENV-Luc and then counter-screening hits with
321 EMC-adapted virus. EMC inhibitors may be a useful chemical tool to study EMC function and also
322 provide a potential antiviral therapeutic against flaviviruses. Host-directed antivirals may have the
323 advantage of a broader activity against multiple viruses and a higher barrier of drug resistance.
324 Only 50% of the adaptation experiments yielded escape mutants containing two mutations after
325 >20 passages. For comparison, for direct-acting antivirals (e.g. viral polymerase inhibitors), one
326 point mutation is often sufficient to overcome the mechanism of action (Beaucourt and Vignuzzi,
327 2014).
328 In addition to characterizing the role of the EMC in the viral life cycle, our data also help to further
329 elucidate its cellular function. The emerging role of the EMC to facilitate membrane protein
330 insertion and biogenesis has been implicated for several cellular transmembrane proteins
331 (Chitwood et al., 2018; Coelho et al., 2019; Guna et al., 2018; Shurtleff et al., 2018; Volkmar et
332 al., 2019). For a subset of tail-anchored proteins, the EMC inserts the sole C-terminal TMD after
333 translation is completed in the cytosol (Guna et al., 2018). Moreover, the EMC co-translationally
334 inserts the first N-terminal TMD of many GPCRs with an N_{exo} topology (N terminus in the ER

335 lumen) (Chitwood et al., 2018). By contrast, we found EMC-dependency within DENV NS4A-4B,
336 a region with several TMDs, which are not close to the termini of the polyprotein. Moreover, as
337 NS4A is already targeted to and inserted into the ER membrane, it argues against an insertase
338 mechanism (as shown for tail-anchored proteins and GPCRs) to ensure NS4B expression. This
339 provides experimental evidence that the EMC is not only capable of supporting stable expression
340 of TMDs near the N and C termini but also of internal TMDs, arguing that the EMC may directly
341 facilitate the biogenesis of a wide variety of implicated transmembrane proteins beyond tail-
342 anchored proteins and GPCRs as suggested previously (Shurtleff et al., 2018). It is noteworthy
343 that the DENV polyprotein is distinct from human transmembrane proteins in that it contains
344 multiple signal peptidase cleavage sites along the polyprotein, including at the 2K/NS4B site
345 between NS4A and NS4B, which removes the 2K peptide acting as signal sequence for NS4B
346 (Lin et al., 1993; Miller et al., 2006). Interestingly, it was shown for ADRB1 that addition of a signal
347 sequence or an N_{cyt} TMD upstream of the first N_{exo} TMD makes the EMC dispensable for
348 biogenesis (Chitwood et al., 2018), whereas NS4B is EMC-dependent despite the upstream 2K
349 signal peptide within the polyprotein. This observation suggests that EMC-mediated
350 integration/stabilization of TMDs may be context-dependent. Generally, for both cellular multi-
351 pass transmembrane proteins and the DENV polyprotein, only one or a subset of TMDs seem to
352 require the EMC for accurate topology, while the other TMDs rely on the Sec61 translocon. The
353 exact interplay between Sec61 and the EMC during transmembrane protein biogenesis warrants
354 further investigation. The simultaneous dependency of flaviviruses on both Sec61 and EMC as
355 highlighted by the CRISPR KO screens could allow an in-depth analysis of the sequence and
356 TMD features that may determine membrane insertion via Sec61 or EMC.
357 Lastly, the EMC was originally discovered to be associated with the UPR (Jonikas et al., 2009),
358 and upregulation of UPR during flavivirus infection has been reported (Peña and Harris, 2011;
359 Reid et al., 2018; Su et al., 2002). It is possible that competition between viral polyproteins and
360 cellular proteins for the machinery important for proper transmembrane protein expression (such

361 as EMC, OST complex and ERAD components) is linked to this phenomenon. The induction of
362 ER stress can further trigger autophagy, which has also been shown to be beneficial for flavivirus
363 infection (Abernathy et al., 2019; Lee et al., 2018; Senft and Ronai, 2015). Therefore, hijacking
364 the EMC may have direct and indirect implications for flavivirus replication.
365 Overall, our study gives detailed insights into how flaviviruses exploit the EMC to support proper
366 polyprotein expression, and we provide further evidence for the cellular function of the EMC in
367 ensuring accurate transmembrane protein topology by utilizing DENV as a cell biological tool.
368

Acknowledgments

We like to thank the following people: Jan Carette for discussions, providing reagents and critically reading the manuscript; Caleb Marceau and Kelsey Hickey for technical advice and providing reagents; members of the Biohub Infectious Disease Initiative and the Weissman lab for discussions and technical advice; the Biohub Genomics Platform for help with sequencing. ASP was supported by the Chan Zuckerberg Biohub. MJS is a Howard Hughes Medical Institute Fellow of the Helen Hay Whitney Foundation and JSW is an Investigator of the Howard Hughes Medical Institute.

378 **Figure legends**

379

380 **Figure 1: EMC is required for flavivirus infection**

381 (A) DENV infection of WT and EMC subunit KO Huh7.5.1 cells. Cells were infected with DENV-
382 Luc, harvested at 30hpi and luminescence was measured. Dotted line indicates background from
383 uninfected control cells.

384 (B) DENV infection of WT and EMC subunit KO HEK293FT cells. Cells were infected with DENV-
385 Luc, harvested at 48hpi and luminescence was measured. Dotted line indicates background from
386 uninfected control cells.

387 (C) Replication of DENV in WT, EMC2- and EMC4-KO, and cDNA complemented KO HEK293FT
388 cells. Cells were infected with DENV-Luc, harvested at 48hpi and luminescence was measured.

389 (D) Quantitative RT-PCR of DENV, WNV, ZIKV and HCV RNA in WT or EMC4-KO Huh7.5.1 cells.
390 Cells were infected with an moi of 0.5 for all viruses and harvested at 30hpi for ZIKV, 48hpi for
391 DENV and WNV, and 72hpi for HCV. Viral RNA levels were normalized to 18S levels and data is
392 displayed relative to the respective WT condition.

393 In all figures, values are shown as mean of three biological replicates with standard deviation in
394 (A)-(C), and as mean with standard error of the mean in (D). *t*-tests were performed to determine
395 statistical significance and *p*-values are defined as ns=non-significant, *<0.05, **<0.01, ***<0.001.

396

397 **Figure 2: EMC is important for optimal viral protein expression**

398 (A) Quantitative RT-PCR of DENV RNA from cell-bound and internalized virions in WT and EMC4-
399 KO Huh7.5.1 cells. Cells were infected on ice with an moi of 30, incubated for 1h, then moved to
400 a 37C incubator, and finally lysed at indicated timepoints. The data are from three biological
401 replicates and shown as mean with standard error of the mean.

402 (B) Luminescence of WT and EMC4-KO HEK293FT cells, which were electroporated with DENV
403 replicon expressing Renilla luciferase and collected at different times post-electroporation. The

404 data are from three biological replicates for each timepoint and shown as mean with standard
405 deviation.
406 (C) Immunoblot analysis of DENV proteins from infected WT and EMC4-KO HEK293FT cells at
407 different timepoints post-infection (6/8/10/12h). Lysates were blotted for different viral proteins
408 (Capsid, NS2B, NS3 and NS5) and GAPDH was used as loading control. UI=uninfected control;
409 L=ladder.
410
411 **Figure 3: EMC knockout does not largely affect viral translation efficiency but leads to**
412 **post-translational protein degradation**
413 (A) Ribosome Profiling (Ribo-seq) and RNA-seq were performed in uninfected WT and EMC4-
414 KO HEK293FT cells to measure changes in translation efficiency (TE). Cycloheximide was added
415 to stop translation and total RNA was isolated. RNA was treated with RNaseI and ribosome-
416 protected footprints were purified, reverse transcribed and amplified for next-generation
417 sequencing. Log_2 fold-change (FC) of reads per kb of transcript, per million mapped reads
418 (RPKMs) between EMC4-KO and WT cells for Ribosome Profiling and RNA-seq are displayed on
419 the y- and x-axis, respectively. Each dot represents one RNA transcript. Fold-change in TE for a
420 given transcript is defined as the change in Ribosome Profiling RPKMs normalized to the change
421 in RNA-seq RPKMs. The red line represents fold-change of TE=1. The Ribosome profiling
422 experiments were performed once for each condition.
423 (B) Ribosome Profiling (Ribo-seq) and RNA-seq were performed in DENV-infected WT and
424 EMC4-KO HEK293FT cells 18h post-infection to measure changes in translation efficiency (TE).
425 The DENV transcript is highlighted in red. The red line represents fold-change of TE=1.
426 (C) Ribosome Profiling (Ribo-seq) and RNA-seq were performed in DENV-infected WT and
427 EMC4-KO HEK293FT cells 44h post-infection to measure changes in translation efficiency (TE).
428 The DENV transcript is highlighted in red. The red line represents fold-change of TE=1.

429 (D) Viral protein expression from DENV infected WT and EMC4-KO HEK293FT cells with or
430 without addition of bortezomib (50nM), a proteasome inhibitor. Cells were harvested at 18hpi and
431 lysates were analyzed by immunoblot using antibodies against dengue proteins. GAPDH was
432 used as loading control. UI=uninfected.
433
434 **Figure 4: EMC is required for proper biogenesis of the NS4A-4B region of the DENV**
435 **polyprotein**
436 (A) Overview of dual-fluorescence reporter constructs of DENV polyprotein for analysis of protein
437 stability. Segments of the DENV genome encoding parts of the polyprotein were cloned with a C-
438 terminal fusion to eGFP-T2A-mCherry (G2C). The T2A peptide leads to peptide bond skipping
439 during translation resulting in two protein products, DENV protein fused to eGFP and mCherry.
440 The GFP:mCherry fluorescence ratio reflects changes in DENV protein stability.
441 (B) GFP:mCherry fluorescence ratio for G2C constructs in WT and EMC4-KO Huh7.5.1 cells.
442 Cells were transfected with G2C construct and analyzed by flow cytometry after 24-48h. For each
443 individual cell the GFP:mCherry ratio was calculated and the fluorescence ratios are depicted as
444 histograms. ADRB1=β1-adrenergic receptor.
445 (C) Measurement of GFP:mCherry fluorescence ratios of NS4A-4B-G2C construct in WT, EMC4-
446 KO and EMC4 cDNA complemented EMC4-KO HEK293FT cells.
447 (D) Measurement of GFP:mCherry fluorescence ratios of NS4A-4B-G2C construct in WT, EMC4-
448 KO and bortezomib-treated EMC4-KO HEK293FT cells. Note that (C) and (D) use same WT and
449 EMC4-KO data as experiments were performed in parallel.
450
451 **Figure 5: Adaptation of DENV to EMC KO cells reveals non-synonymous point mutations**
452 **in NS4A and NS4B**
453 (A) Identification of SNPs in EMC4-KO adapted DENV relative to DENV 16681 reference genome
454 by next-generation sequencing of supernatant-extracted viral RNA. DENV was serially passaged

455 on EMC4 KO Huh7.5.1 cells every 3-4 days. After 20-22 passages supernatant was collected and
456 RNA extracted from three independent passaging experiment. Truseq total RNA sequencing
457 libraries were generated and reads were mapped to the reference genome. Mutations common
458 across all three replicates are highlighted by red boxes and their nucleotide and amino acid
459 changes are shown below. A table of all identified SNPs can be found in Figure 5 - figure
460 supplement 1).
461 (B) Viral growth curves of WT and EMC-adapted DENV in WT and EMC4 KO cells measured by
462 quantitative RT-PCR. Cells were infected with WT or EMC-adapted virus at an moi of 0.5 and
463 harvested at indicated timepoints. The data are from three biological replicates and shown as
464 mean with standard error of the mean.
465 (C) Viral replication of WT DENV-Luc or mutant DENV-Luc (containing A6665G and A7558T
466 either individually or in tandem) in EMC4 KO cells relative to WT cells. Lysates were collected
467 72hpi and luminescence was measured. The data are from three biological replicates and shown
468 as mean with standard deviation.
469 (D) Measurement of GFP:mCherry fluorescence ratios of WT NS4A-5-G2C and NS4A-
470 5(A6665G,A7558T)-G2C constructs in WT and EMC4-KO Huh7.5.1.
471
472 **Figure 6: EMC physically interacts with DENV NS4B post-cleavage and knockout of EMC**
473 **leads to an aberrant topology of NS4A and NS4B**
474 (A) Immunoblot for processed products of transfected NS2B-4B-GFP construct in WT and EMC4
475 KO cells in presence or absence of BZ. Anti-GFP antibody was used to detect processed viral
476 proteins and p84 was used as loading control.
477 (B) Co-immunoprecipitation of EMC4-FLAG from lysates of uninfected (UI) or DENV infected
478 HEK293FT EMC4-FLAG cells. Cells were harvested after 96h and lysates were incubated with
479 anti-FLAG magnetic beads. Eluates were immunoblotted for different viral proteins (prM, NS4B,
480 NS5). p84 was used as loading and non-specific binding control.

481 (C) Co-immunoprecipitation of EMC4-FLAG from lysates of uninfected cells (UI), cells infected
482 with WT DENV (WT) or infected with EMC adapted DENV (AD).
483 (D) Protease protection assay for different NS4A-4B-eGFP fusion constructs. Experimentally
484 determined topology according to (Miller et al., 2006, 2007) and generated constructs are
485 displayed. Different shades of blue indicate NS4A, 2K and NS4B in den model and red triangle
486 points to signal peptidase cleavage site. Constructs were transfected into WT or EMC4-KO cells.
487 After 24-48h cell pellets were resuspended in buffer with digitonin, and subsequently treated with
488 proteinase K (PK) or left untreated. Finally, samples were lysed and immunoblotted using anti-
489 GFP antibody.
490 (E) Deglycosylation assay using PNGase F to probe luminal localization of NS4A TMD2 using
491 constructs containing the NS4A WT sequence or A6665G mutation. Opsin tags containing a N-
492 K-T sequon were inserted downstream of NS4A TMD2. WT or EMC4-KO cells were transfected
493 with WT or mutant construct and harvested after 24h. Lysates were treated with PNGase F to
494 remove N-linked oligosaccharides or left untreated following analysis by immunoblot using anti-
495 FLAG antibody. Upper bands represent NS4A with glycosylated and thus luminally localized opsin
496 tag while lower bands are non-glycosylated forms.
497 (F) Possible model for the role of EMC in flavivirus infection. In infected WT cells, the EMC co-
498 translationally engages with NS4A and NS4B TMDs to facilitate or maintain correct insertion and
499 topology of TMDs ensuring stable expression. In the absence of the EMC, the correct topology is
500 not obtained during biogenesis, leading to misfolding and degradation of the NS4A-4B viral
501 proteins.
502
503 **Figure 1 - figure supplement 1: Genotyping and flavivirus infection of EMC KO cell lines**
504 (A) Sanger sequencing of clonal EMC subunit KO Huh7.5.1 and HEK293FT cells. sgRNA
505 targeting site is highlighted in reference sequence (top) and indel mutation is shown below

506 sequencing trace of KO cells. For heterozygous mutants, TIDE was used to determine indel
507 mutations.
508 (B) Timecourse of DENV infection in WT or EMC2-KO Huh7.5.1 at 30, 48 and 72h post infection.
509 Cells were lysed and viral RNA was quantified by RT-PCR. Values are normalized to 18S RNA
510 and shown relative to the WT, 30h condition.
511 (C) Immunoblot analysis of EMC2 or EMC4 expression in WT, EMC2- and EMC4-KO, and cDNA
512 complemented KO HEK293FT cells. p84 was used as loading control.
513 (D) Quantitative RT-PCR of DENV, WNV and ZIKV RNA in WT or EMC4-KO HEK293FT cells.
514 For QPCR experiments, values are shown as mean of three biological replicates with standard
515 error of the mean.
516
517 **Figure 2 - figure supplement 1: EMC directly affects viral protein expression and not**
518 **genome replication**
519 (A) Luminescence of WT and EMC4-KO cells electroporated with DENV replicon expressing
520 Renilla luciferase and treated with MK-0608 (a nucleoside analogue, which inhibits the DENV
521 polymerase) or DMSO. Lysates were collected at different times post electroporation. The data
522 are from three biological replicates and shown as mean with standard deviation.
523 (B) Immunoblot analysis of DENV infected WT and EMC4-KO HEK293FT cells at different
524 timepoints post-infection (6/8/10/12h) with treatment of MK-0608 to inhibit viral replication.
525 Lysates were blotted for different viral proteins (Capsid, NS2B, NS3 and NS5) and GAPDH was
526 used as loading control. UI=uninfected control; L=ladder.
527
528 **Figure 3 - figure supplement 1: DENV efficiently translates and produces full-length**
529 **polyproteins in EMC KO cells**

530 (A) Translation efficiencies (number of ribosomal footprints normalized to the number of RNAseq
531 reads) of cellular mRNA and DENV RNA in WT and EMC4-KO cells at 18 and 44hpi. DENV is
532 highlighted as red dot.
533 (B) Footprint distribution of Ribosome Profiling reads mapped to the DENV genome in WT and
534 EMC4-KO cells at 18 and 44hpi. Nucleotide position of DENV genome is indicated on x-axis.
535
536 **Figure 3 - figure supplement 2: Bortezomib-recovered viral proteins do not restore viral**
537 **replication**
538 DENV-Luc infection of WT and EMC4 KO HEK293FT cells treated with DMSO control or different
539 concentrations of BZ. Cells were harvested at 24hpi and luminescence was measured. Dotted
540 line indicates background signal from uninfected cells.
541
542 **Figure 4 - figure supplement 1: EMC is required for proper biogenesis of the NS4A-4B**
543 **region of the DENV polyprotein in HEK293 cells**
544 GFP:mCherry fluorescence ratio for G2C constructs in WT and EMC4-KO HEK293FT cells. Cells
545 were transfected with G2C construct and analyzed by flow cytometry after 24-48h. For each
546 individual cell the GFP:mCherry ratio was calculated and the fluorescence ratios are depicted as
547 histograms. ADRB1=β1-adrenergic receptor.
548
549 **Figure 5 - figure supplement 1: Identified SNPs in EMC KO adapted DENV isolates**
550 Table containing all identified SNPs from the three isolated EMC-adapted viruses relative to the
551 DENV 16681 reference genome. A minimum variant frequency cutoff of 80% was used.
552
553

554 **Figure 5 - figure supplement 2: DENV containing EMC KO adapted mutations efficiently**
555 **replicates in EMC deficient cells**

556 (A) Quantitative RT-PCR of DENV RNA from WT DENV 16681 and the three isolated EMC-
557 adapted DENV in WT and EMC4 KO Huh7.5.1. Cells were infected with an moi of 0.5 and
558 harvested 48hpi. Viral RNA was normalized to 18S RNA and values are displayed relative to the
559 respective WT cell condition. The data are from three biological replicates and shown as mean
560 with standard error of the mean.

561 (B) Timecourse infection experiment with WT, A6665G and A665G/A7558T DENV-Luc in WT or
562 EMC4 KO Huh7.5.1. Cells were infected, lysates harvested at 24, 48 and 72 hpi and
563 luminescence was measured. The data are from three biological replicates and shown as mean
564 with standard deviation.

565

566 **Material and methods**

Key Resources Table				
Reagent type (species) or resource	**Designation**	**Source or reference**	**Identifiers**	**Additional information**
Cell line (human)	HEK293FT	ThermoFisher	R70007	
Cell line (human)	EMC1-KO HEK293FT	This study		See Material and Methods, “Generation of knockout cell lines”
Cell line (human)	EMC2-KO HEK293FT	This study		See Material and Methods, “Generation of knockout cell lines”
Cell line (human)	EMC3-KO HEK293FT	This study		See Material and Methods, “Generation of knockout cell lines”
Cell line (human)	EMC4-KO HEK293FT	This study		See Material and Methods, “Generation of knockout cell lines”
Cell line (human)	EMC5-KO HEK293FT	This study		See Material and Methods, “Generation of knockout cell lines”
Cell line (human)	Huh7.5.1	PMID: 15939869	RRID: CVCL_E049	
Cell line (human)	EMC1-KO HUH7.5.1	This study		See Material and Methods, “Generation of knockout cell lines”

Cell line (human)	EMC2-KO HUH7.5.1	This study		See Material and Methods, “Generation of knockout cell lines”
Cell line (human)	EMC3-KO HUH7.5.1	This study		See Material and Methods, “Generation of knockout cell lines”
Cell line (human)	EMC4-KO HUH7.5.1	This study		See Material and Methods, “Generation of knockout cell lines”
Cell line (human)	EMC5-KO HUH7.5.1	This study		See Material and Methods, “Generation of knockout cell lines”
Cell line (human)	EMC6-KO HUH7.5.1	This study		See Material and Methods, “Generation of knockout cell lines”
Biological sample (virus)	DENV serotype 2 strain 16681	PMID: 9143286	NCBI Reference Sequence: NC_001474.2	Generated from infectious clone obtained from Karla Kirkegaard
Biological sample (virus)	DENV-Luc	PMID: 27383987		
Biological sample (virus)	WNV Kunjin strain CH16532	Other	GenBank: JX276662.1	Source: John F. Anderson
Biological sample (virus)	ZIKV PRVABC59	BEI Resources	NR-50240	
Biological sample (virus)	HCV JFH1	PMID: 11424123	GenBank: AB047639.1	

Antibody	P84 (mouse, monoclonal)	Genetex	GTX70220	1:2000
Antibody	GAPDH (mouse, monoclonal)	SCBT	sc-32233	1:2000
Antibody	EMC2/TTC35 (rabbit, polyclonal)	Proteintech	25443-1-AP	1:750
Antibody	EMC4 (rabbit, polyclonal)	Bethyl	A305-752A	1:500
Antibody	Dengue virus prM protein (rabbit, polyclonal)	Genetex	GTX128093	1:1000
Antibody	Dengue virus capsid protein (rabbit, polyclonal)	Genetex	GTX103343	1:1000
Antibody	Dengue virus NS2B (rabbit, polyclonal)	Genetex	GTX124246	1:1000
Antibody	Dengue virus NS3 protein (mouse, monoclonal)	Genetex	GTX629477	1:1000
Antibody	Dengue virus NS4B protein (rabbit, polyclonal)	Genetex	GTX124250	1:1000
Antibody	Dengue virus Type 2 NS5 protein (mouse, monoclonal)	Genetex	GTX629447	1:1000

Antibody	GFP (rabbit, polyclonal)	Genetex	GTX113617	1:5000
Antibody	FLAG (mouse, monoclonal)	Sigma	F1804	1:2000
recombinant DNA reagent	EMC2 cDNA	GenScript	clone OHu30604	
recombinant DNA reagent	EMC4 cDNA	GenScript	clone OHu00964	
commercial assay or kit	Renilla Luciferase Assay system	Promega	E2810	
commercial assay or kit	Power SYBR Cells-to-CT kit	ThermoFisher	4402953	
chemical compound, drug	MK-0608 (2'-C-Methylcytidine)	Carbosynth	NM07918	working concentration: 25 μM
chemical compound, drug	Bortezomib	Selleckchem	S1013	working concentration: 1-50 nM
chemical compound, drug	Cycloheximide	Sigma	C7698	working concentration: 100 μg/ml
software, algorithm	Prism 8	GraphPad		

software, algorithm	FlowJo	FlowJo		

567

568 ***Cell culture and viruses***

569 Huh7.5.1 (obtained from Peter Sarnow, original gift from Frank Chisari) and HEK293FT (Thermo
570 Scientific) were cultured in DMEM (Gibco) supplemented with 10% fetal bovine serum (Omega
571 Scientific), penicillin/streptomycin (Gibco), non-essential amino acids (Gibco) and L-glutamine
572 (Gibco) at 37C and 5% CO_2. Parental cell lines were tested negative for mycoplasma and were
573 authenticated by STR profiling. The following virus strains were used: DENV serotype 2 strain
574 16681 (stocks kindly provided by Caleb Marceau), DENV-Luc (stocks kindly provided by Jan
575 Carette) (Marceau et al., 2016), WNV Kunjin strain CH16532 (stocks kindly provided by Jan
576 Carette), ZIKV PRVABC59 (stocks kindly provided by Jan Carette) and HCV JFH1 (stocks kindly
577 provided by Jan Carette). Viral titers were determined by plaque- or focus-forming assay.

578

579 ***Chemical compounds***

580 MK-0608 (2'-C-Methylcytidine) was purchased from Carbosynth and used at a concentration of
581 25 µM. Bortezomib was obtained from Selleckchem and used at concentrations 1-50 nM. For all
582 experiments, DMSO controls were included. Cycloheximide was purchased from Sigma and used
583 at 100 µg/ml for Ribosome Profiling experiments.

584

585 ***Generation of knockout cell lines***

586 Oligos containing sgRNA sequence were annealed and ligated into pX458 (gift from Feng Zhang;
587 Addgene plasmid # 48138). Cells were transfected with pX458 using Lipofectamine 3000
588 (Invitrogen) and two days later GFP positive cells were single-cell sorted into 96-well plates using
589 a Sony SH800 cell sorter. For genotyping, genomic DNA was isolated from obtained clones using

590 QuickExtract (Lucigen), the sgRNA-targeted sites PCR amplified and the products Sanger-
591 sequenced. Obtained sequences were compared to reference sequences for indel mutations. In
592 the case of heterozygous mutations, TIDE was used to deconvolute sequencing traces (Brinkman
593 et al., 2014). A list of all used sgRNA oligo and genotyping primer sequences can be found in
594 Supplementary Table 1.
595
596 ***Dengue Luciferase assay***
597 Huh7.5.1 or HEK293FT cells were seeded in 96-well plates and infected with DENV-Luc at an
598 moi of 0.01. Cells were harvested in Renilla Lysis buffer and luminescence was measured using
599 Renilla Luciferase Assay system (Promega) on a Spectramax i3x Multi-Mode Microplate Reader
600 (Molecular Devices).
601
602 ***Quantitative RT-PCR***
603 Huh7.5.1 or HEK293FT cells were plated in 96-well plates (in triplicates for each condition) and
604 infected with an moi of 0.5 for all viruses. Cells were then harvested at 30hpi for ZIKV, 48hpi for
605 DENV and WNV, and 72hpi for HCV using the Power SYBR Cells-to-CT kit (Invitrogen). After
606 reverse transcription, quantitative PCR was performed on a Bio-Rad CFX96 Touch system. All
607 viral RNA levels were normalized to 18S levels. For viral internalization assay, 96-well plates
608 containing WT or EMC4 KO Huh7.5.1 cells were put on ice before infection with DENV at an moi
609 of 30. Cells were incubated for 1h before moving them to a 37C incubator. At each harvest
610 timepoint, cells were washed three times with PBS and lysed as described above. All qPCR primer
611 sequences can be found in Supplementary Table 1.
612
613 ***Lentiviral complementation***
614 EMC2 (GenScript; clone OHu30604) and EMC4 cDNA (GenScript; clone OHu00964) were PCR
615 amplified using tgtggtggaattctgcagataccATGGCGAAGGTCTCAGA /

616 CGGCCGCCACTGTGCTGGATTTACTTATCGTCGTCATCCTTGTAATCAGACTGGGTGATC
617 and tgtggtggaattctgcagataccATGACGGCCCAGGGG /
618 CGGCCGCCACTGTGCTGGATTTACTTATCGTCGTCATCCTTGTAATCCAAAAGCAGTCCT,
619 respectively, and cloned into EcoRV-cut pLenti CMV Puro DEST (w118-1) (gift from Eric
620 Campeau & Paul Kaufman; Addgene plasmid # 17452) using NEBuilder® HiFi DNA Assembly
621 Master Mix (New England BioLabs). Lentivirus was produced in HEK293FT, respective KO cells
622 transduced with filtered, lentiviral containing supernatant and selected using 2-4 µg/ml puromycin
623 (Gibco) for 3-4 days.
624
625 ***Replicon assay***
626 DENV replicon plasmid (Marceau et al., 2016) was linearized using XbaI restriction enzyme.
627 Replicon RNA was generated using the MEGAscript T7 Kit (Invitrogen) with the reaction
628 containing 5mM m7G(5')ppp(5')G RNA Cap Structure Analog (New England BioLabs). Resulting
629 RNA was purified by lithium chloride precipitation. For electroporation, 2 million WT or EMC4 KO
630 HEK293FT cells were washed twice in PBS, resuspended in 100 µl SF Nucleofector solution
631 (Lonza), mixed with 4 µg replicon RNA, transferred to a 100ul nucleocuvette and pulsed using
632 program CM-130 on an Amaxa 4D-Nucleofector™ X Unit (Lonza). Cells were then resuspended
633 in antibiotic-free medium, distributed into 96-wells and lysed at different timepoints post-
634 electroporation using Renilla Lysis buffer. Luminescence was measured using Renilla Luciferase
635 Assay system (Promega) on a Spectramax i3x Multi-Mode Microplate Reader (Molecular
636 Devices).
637
638 ***Immunoblotting***
639 Cell were lysed using Laemmli SDS sample buffer containing 5% beta-mercaptoethanol and
640 boiled for 10min. Lysates were separated by SDS-PAGE on pre-cast Bio-Rad 4-15% poly-
641 acrylamide gels in Bio-Rad Mini-Protean electrophoresis system. Proteins were transferred onto

642 PVDF membranes using Bio-Rad Trans-Blot Turbo transfer system. PVDF membranes were
643 blocked with PBS buffer containing 0.1% Tween-20 and 5% non-fat milk. Blocked membranes
644 were incubated with primary antibody diluted in blocking buffer and incubated overnight at 4C on
645 a shaker. Primary antibodies were detected by incubating membranes with 1:10000 dilution of
646 HRP-conjugated (Southern Biotech) or IRDye-conjugated (LI-COR) secondary anti-mouse and
647 anti-rabbit antibodies for 1 h at room temperature. Blots were visualized using a ChemiDoc™ MP
648 Imaging System (Bio-Rad). The following primary antibodies (and their dilutions) were used in
649 this study: p84 (Genetex, GTX70220) at 1:2000, GAPDH (SCBT, sc-32233) at 1:2000,
650 EMC2/TTC35 (Proteintech, 25443-1-AP) at 1:750, EMC4 (Bethyl, A305-752A) at 1:500, Dengue
651 virus prM protein (Genetex, GTX128093) at 1:1000, Dengue virus Capsid protein (Genetex,
652 GTX103343) at 1:1000, Dengue virus NS2B (Genetex, GTX124246) at 1:1000, Dengue virus NS3
653 protein (Genetex, GTX629477) at 1:1000, Dengue virus NS4B protein (Genetex, GTX124250) at
654 1:1000, Dengue virus Type 2 NS5 protein (Genetex, GTX629447), GFP (Genetex, GTX113617)
655 at 1:5000 and FLAG M2 (Sigma, F1804) at 1:2000.
656
657 ***Ribosome profiling***
658 WT and EMC4 KO HEK293FT were plated in 10cm dishes and infected with DENV at an of 100
659 for the 18hpi harvest and an moi of 0.5 for the 44hpi harvest. Cells were treated with 100 µg/ml
660 cycloheximide for 2 min, washed once with polysome gradient buffer (20 mM Tris pH 7.5, 150
661 mM NaCl, 5 mM $MgCl_2$, 100 µg/mL cycloheximide, 1 mM DTT) and then lysed using 500 µl of
662 polysome lysis buffer (20 mM Tris pH 7.5, 150 mM NaCl, 5 mM $MgCl_2$, 1% Triton X-100, 1 mM
663 DTT, 100 µg/mL cycloheximide, 24 U/ml Turbo DNase (Ambion)) per plate. Cells/lysates were
664 collected using cell scrapers and incubated on ice for 15min. Crude lysates were centrifuged at
665 20,000 x g for 2 min at 4C and the cleared polysome-containing lysates flash frozen by immersion
666 in liquid nitrogen and stored at -80C until further processing. For ribosomal footprinting, 30 µg
667 total RNA diluted in polysome buffer to a total volume of 200µl were treated with 750 U/ml RNaseI

668 (Ambion) for 45min at 25C with shaking (300rpm). RNase activity was quenched by adding 10ul
669 SuperaseIN (Invitrogen) and placing samples on ice. Note that 10% of the lysates were saved for
670 RNA-seq library preparation (see below). A 1ml sucrose cushion was added to the bottom of a
671 13mm x 56mm thick-wall polycarbonate tube (Beckman Coulter) for each sample and the footprint
672 digests were layered on top. Tubes were ultracentrifuged at 100,000 rpm for 4h at 4C in a
673 TLA100.3 rotor (Beckman Coulter). After spin, supernatant was removed and the monosome-
674 containing pellet was resuspended in 300 µl Trizol LS (Life Technologies) for RNA extraction
675 using the Direct-Zol kit (Zymo). Ribosome Profiling NGS libraries were generated as previously
676 described (Shurtleff et al., 2018).
677 For corresponding RNA-seq libraries RNA was extracted from the remaining undigested cleared
678 lysates using Trizol and the Direct-Zol kit. 1 µg purified total RNA was used as input for the Truseq
679 stranded total RNA Gold library prep (Illumina). Ribosomal RNA was depleted using Ribo-Zero
680 H/M/R Gold and depleted RNA fragmented for 8min at 94C. Following first and second strand
681 synthesis products were purified using SPRI beads. KAPA dual-indexed adapters (Kapa
682 Biosystems, KK8722) were used for adapter ligation. Finally, PCR enriched products were
683 cleaned up using SPRI. Ribosome Profiling and RNA-seq libraries were analyzed on Bioanalyzer
684 or TapeStation (Agilent) before sequencing on a NextSeq 500 platform (Illumina) in separate runs
685 with 400M reads output.
686
687 ***Analysis of Ribosome Profiling data***
688 Reads from Ribosome Profiling or RNA-seq were preprocessed by removing low-quality reads
689 and trimming of adaptor sequences. Next, ribosomal RNA reads were removed using Bowtie.
690 Remaining reads were aligned to the human reference genome file also containing the genomic
691 DENV2 16681 sequence using Tophat to generate read count tables with RPKMs for each
692 transcript. A cutoff of at least 5 RPKMs was used for further analysis of transcripts/footprint counts,
693 and $\log_2$ fold-changes (FC) were calculated between corresponding EMC4 KO and WT samples

694 for both Ribosome Profiling and RNA-seq. To calculate translation efficiency (TE), the Ribosome
695 Profiling RPKMs were normalized by the RNA-seq RPKMs for each transcript.
696 To analyze the footprint distribution of Ribosome Profiling reads across the DENV genome, DENV
697 specific reads were mapped to the DENV2 16681 reference sequence using Geneious Prime and
698 coverage at each nucleotide position was determined.
699
700 ***Dual fluorescence cytometry assay***
701 eGFP was amplified from pX458 with adding overhang to plenti-CMV-Puro (EcoRV cut site), a
702 Kozak sequence and ATG start codon for the G2C-only construct or with an additional overhang
703 to GlySer-linker sequence for fusion with DENV fragments. T2A-mCherry was amplified from
704 pX458 where eGFP had been replaced with mCherry. Different regions of the DENV genome
705 were amplified from the DENV2 16681 infectious clone plasmid (gift from Karla Kirkegaard) with
706 addition of overhang sequences to plenti-CMV backbone, Kozak sequence and ATG start codon
707 on 5'end and to GlySer-linker-GFP fragment on 3'end. ADRB1 was amplified from pcDNA3 Flag
708 beta-1-adrenergic-receptor (gift from Robert Lefkowitz; Addgene plasmid # 14698). All fragments
709 contained ~20bp overhangs and were assembled into EcoRV cut pLenti CMV Puro DEST (w118-
710 1) using NEBuilder® HiFi DNA Assembly Master Mix (New England BioLabs) or Gibson-like
711 master mix (Berkeley MacroLabs) to generate G2C reporter expression constructs. All constructs
712 were verified by Sanger sequencing. Primer sequences can be found in Supplementary Table 1.
713 For the G2C dual fluorescence assay, cells were seeded in 24- or 12-well plates and transfected
714 with G2C constructs using Lipofectamine 3000 (Invitrogen). 24-48h later cells were trypsinized,
715 filtered (70µm), and analyzed by flow cytometry using a Cytoflex S flow cytometer (Beckman
716 Coulter). At least 5,000 and 10,000 mCherry positive cells were recorded for Huh7.5.1 and
717 HEK293FT, respectively. For analysis, cells were gated based on FSC/SSC, FSC-H/FSC-A
718 (singlets) and finally ECD (mCherry) and FITC (eGFP) using FlowJo 10. Raw fluorescence data
719 for all gated fluorescent cells were exported and the eGFP:mCherry intensity ratios were

720 calculated for individual cells. All fluorescence ratios were normalized to the mean of the G2C-
721 only construct. Distributions of fluorescence ratios were plotted as histograms using GraphPad
722 Prism 8.
723
724 ***Viral adaptation***
725 WT DENV serotype 2 strain 16681 was serially passaged every 3-4 days onto newly plated EMC4
726 KO Huh7.5.1 cells by transferring increasingly diluted supernatant from infected cells (starting at
727 2-fold dilutions for the first 3 passages, then stepwise increase of dilutions to 100-fold for the final
728 passages). Six independent passaging experiments were started and cytopathic effects were
729 observed in three of the replicates after approximately 20-22 passages. Supernatant was then
730 harvested, filtered through a 0.45 um filter to remove cellular debris, and RNA was extracted using
731 Trizol LS and Direct-Zol kit (Zymo). Additionally, RNA was extracted from WT DENV stock. To
732 prepare sequencing libraries, Truseq stranded total RNA Gold library kit (Illumina) was used.
733 Isolated RNA was fragmented for 4min at 94C without prior Ribo-Zero depletion, followed by first
734 and second strand synthesis, and adapter ligation. Fragments were amplified in presence of
735 SYBR Green on Bio-Rad CFX96 and reaction was stopped for each sample before it reached
736 plateau (~20-24 cycles). Libraries from different virus isolates were pooled and sequenced on
737 iSeq 100 (Illumina) with 2x75bp reads.
738 For analysis, Geneious Prime was used: Fastq files were imported as paired reads and Truseq
739 adapters and low-quality sequences (minimum 20) were trimmed using BBDuk. Next, reads were
740 mapped to the WT 16681 reference genome using the Geneious Mapper at medium-low
741 sensitivity and with 5 iterations for fine-tuning. All samples had a minimum coverage of 1000 at
742 all nucleotide positions. Finally, SNPs between adapted and WT stock viruses were called with a
743 minimum variance frequency of 80%. To compare acquired non-synonymous point mutations to
744 a large dataset of sequenced DENV2 strains, 1,359 complete genome sequences from NCBI
745 were mapped to the DENV2 16681 strain containing adapted mutations.

746

747 ***Generation of EMC adapted DENV-Luciferase***

748 DENV-Luc infectious clone containing adapted mutations were generated by PCR amplification
749 from WT DENV-Luc infectious clone plasmid (gift from Jan Carette). For DENV-Luc(A6665G)
750 fragments were amplified using GAAGAGTGATGGTTATGGTAGGC /
751 CTGTATTTGTGCGCACCATAGGAGGATG and CATCCTCCTATGGTGCGCACAAATACAG /
752 GTGATCTTCATTTAAGAATCCTAGGGCTTC. For DENV-Luc(A7558T) fragments were
753 amplified using GAAGAGTGATGGTTATGGTAGGC / CCCCTTCTTGTGTAGGTTGTGTTCTTC
754 and GAAGAACACAACCTACACAAGAAGGGG / GTGATCTTCATTTAAGAATCCTAGGGCTTC.
755 For DENV-Luc(A6665G, A7558T) fragments were amplified using
756 GAAGAGTGATGGTTATGGTAGGC / CTGTATTTGTGCGCACCATAGGAGGATG,
757 CATCCTCCTATGGTGCGCACAAATACAG / CCCCTTCTTGTGTAGGTTGTGTTCTTC, and
758 GAAGAACACAACCTACACAAGAAGGGG / GTGATCTTCATTTAAGAATCCTAGGGCTTC.
759 PCR products were cloned into NarI and AvrII cut WT DENV-Luc infectious clone using
760 NEBuilder® HiFi DNA Assembly Master Mix (New England BioLabs) and transformed into Stbl3
761 bacteria (Berkeley MacroLabs). Constructs were verified by Sanger sequencing. Plasmids were
762 linearized with XbaI and RNA was generated by in-vitro transcription using the MEGAscript T7 Kit
763 (Invitrogen) with the reaction containing 5mM m7G(5')ppp(5')G RNA Cap Structure Analog (New
764 England BioLabs). Resulting RNA was purified by lithium chloride precipitation and transfected
765 into BHK-21 cells using Lipofectamine 3000 for viral production. Supernatants were harvested 6-
766 9 days post-transfection.

767

768 ***Focus-forming unit assay***

769 Huh7.5.1 cells were seeded in 24-well plates. Next day, cells were infected with DENV stocks at
770 serial dilutions from 10^{-1} to 10^{-6} in a total volume of 500 µl. 30 h later, cells were fixed with 4%
771 PFA in PBS. Cells were washed three times with PBS and then blocked for 15 min at room

772 temperature in blocking buffer (PBS containing 1% saponin, 1% Triton X-100, 5% fetal bovine
773 serum, and 0.1% azide). Fixed cells were incubated with mouse 4G2 antibody (Novusbio, # D1-
774 4G2-4-15) diluted 1:1000 in blocking buffer for 1 hour with gentle shaking. Primary antibody was
775 washed off with three PBS washes and then cells were incubated with Alexa-Fluor 488 anti-
776 mouse antibody (Life Technologies) diluted 1:1000 for 30 min. Secondary antibody was washed
777 off with two PBS washes. Lastly, cells were stained with Hoechst diluted 1:2000 in PBS and
778 fluorescent colonies were counted under the microscope.
779
780 ***Co-immunoprecipitation***
781 HEK293FT EMC4 KO cells complemented with FLAG-tagged EMC4 were seeded in a 10cm dish
782 and infected with DENV (moi=1) for 96h. Cells were washed with PBS and then collected in 1ml
783 Pierce RIPA buffer (Thermo Scientific) containing 1mM PMSF (Thermo Scientific), 5mM EDTA
784 and 1x Halt Protease Inhibitor Cocktail (Thermo Scientific) with help of cell scrapers. Cells were
785 lysed on ice for 1h with occasional vortexing and subsequently centrifuged at 15,000 x g for 10min
786 at 4C to clear lysates. For co-immunoprecipitation, clarified lysates were incubated at 4C
787 overnight with Anti-FLAG® M2 Magnetic Beads (Sigma) while rotating. Beads were washed three
788 times using TBS-T and eluted by boiling in 2x Laemmli buffer. Eluates were loaded for SDS-PAGE
789 and stained for viral proteins.
790
791 ***Protease protection assay***
792 NS4A-4B was amplified starting from NS4A and ending as indicated in Figure 6D with addition of
793 an upstream overhang to plenti-CMV-Puro, a Kozak sequence and ATG start codon, and a
794 downstream overhang to eGFP. Fragments were assembled into EcoRV-cut plenti-CMV-Puro
795 using Gibson-like master mix (Berkeley MacroLabs). Plasmids were then transfected into WT and
796 EMC4 KO cells, trypsinized after 24h and pelleted by centrifugation at 400xg for 5min. Pellets
797 were resuspended in PBS, split into two tubes and pelleted again. Pellets were either

798 resuspended in KHM buffer (110 mM potassium acetate, 20 mM HEPES, 2 mM $MgCl_2$) or KHM
799 buffer containing 50 µM digitonin (Sigma) and 50 µg/ml proteinase K (Qiagen) and incubated on
800 ice for 45min. Subsequently, PMSF (Sigma) was added to a final concentration of 10 mM. After
801 10min, 2x Laemmli buffer containing 5% beta-mercaptoethanol was added and samples were
802 boiled for 10min. Lysates were analyzed by immunoblotting as described above using the anti-
803 GFP antibody.
804
805 ***Deglycosylation assay***
806 An opsin tag with the amino acid sequence GPNFYVPFSNKTG (containing a sequon for N-
807 glycan) (Buentzel and Thoms, 2017) was introduced downstream of NS4A TMD2 at amino acid
808 position 99 of NS4A. Constructs contained either the WT sequence or the A6665G mutation and
809 were FLAG-tagged at the N-terminus of NS4A. WT and EMC4 KO cells were transfected,
810 harvested in Pierce RIPA buffer (Thermo Scientific) containing 1x Halt Protease Inhibitor Cocktail
811 (Thermo Scientific) after 24h, and deglycosylation assay was performed using PNGase F (New
812 England BioLabs) according to the manufacturer's instructions. Briefly, lysates were mixed with
813 Glycoprotein Denaturing Buffer and incubated at 98C for 10min. Subsequently, 10% NP-40 and
814 GlycoBuffer 2 were added, samples split in halve and incubated at 37C for 1.5h with or without
815 PNGase F. Finally, 4x Laemmli buffer containing 5% beta-mercaptoethanol was added, samples
816 were boiled for 10min and analyzed by immunoblotting using anti-FLAG M2 antibody (Sigma).
817
818 ***Statistical analysis and reproducibility***
819 GraphPad Prism 8 was used to analyze data and perform statistical tests. Unpaired *t*-tests were
820 applied to measure statistical significance of differences in DENV infection between WT and EMC
821 KO cells. Infection experiments were performed with three biological replicates each. Biological
822 replicates are defined as independent infections and measurements of separate wells. Each set
823 of infection experiments containing three biological replicates was repeated twice and one

824 representative is shown in the figures. Immunoblot and flow cytometry experiments were
825 performed at least twice and one representative is shown.
826
827

828 **Supplementary tables**

829 ***Figure 3 – Source Data 1***

830 Ribosome Profiling data including read counts and fold changes for ribosome footprints and RNA-
831 seq used to generate Figures 3A-C.

832

833 ***Supplementary Table 1***

834 Table of oligos used in this study: sgRNA oligos, genotyping primers, qPCR primers, primers to
835 generate G2C constructs

836

837 **Data availability**

838 Fastq files of Ribosome Profiling and RNA-seq experiments have been deposited in the Sequence
839 Read Archive (SRA) of NCBI under the accession code PRJNA526529.

840 **References**

841 Abernathy, E., Mateo, R., Majzoub, K., van Buuren, N., Bird, S.W., Carette, J.E., and
842 Kirkegaard, K. (2019). Differential and convergent utilization of autophagy components by
843 positive-strand RNA viruses. PLoS Biol. *17*, e2006926.

844 Beaucourt, S., and Vignuzzi, M. (2014). Ribavirin: a drug active against many viruses with
845 multiple effects on virus replication and propagation. Molecular basis of ribavirin resistance.
846 Curr. Opin. Virol. *8*, 10–15.

847 Brinkman, E.K., Chen, T., Amendola, M., and van Steensel, B. (2014). Easy quantitative
848 assessment of genome editing by sequence trace decomposition. Nucleic Acids Res. *42*, e168–
849 e168.

850 Buentzel, J., and Thoms, S. (2017). The Use of Glycosylation Tags as Reporters for Protein
851 Entry into the Endoplasmic Reticulum in Yeast and Mammalian Cells. In Peroxisomes: Methods
852 and Protocols, M. Schrader, ed. (New York, NY: Springer New York), pp. 221–232.

853 Cahour, A., Falgout, B., and Lai, C.-J. (1992). Cleavage of the Dengue Virus Polyprotein at the
854 NS3/NS4A and NS4B/NS5 Junctions Is Mediated by Viral Protease NS2B-NS3, Whereas
855 NS4A/NS4B May Be Processed by a Cellular Protease. J VIROL *66*, 8.

856 Chen, Y.-L., Yokokawa, F., and Shi, P.-Y. (2015). The search for nucleoside/nucleotide analog
857 inhibitors of dengue virus. Antiviral Res. *122*, 12–19.

858 Chitwood, P.J., and Hegde, R.S. (2019). The Role of EMC during Membrane Protein
859 Biogenesis. Trends Cell Biol.

860 Chitwood, P.J., Juszkiewicz, S., Guna, A., Shao, S., and Hegde, R.S. (2018). EMC Is Required
861 to Initiate Accurate Membrane Protein Topogenesis. Cell *175*, 1507-1519.e16.

862 Christianson, J.C., Olzmann, J.A., Shaler, T.A., Sowa, M.E., Bennett, E.J., Richter, C.M., Tyler,
863 R.E., Greenblatt, E.J., Harper, J.W., and Kopito, R.R. (2011). Defining human ERAD networks
864 through an integrative mapping strategy. Nat. Cell Biol. *14*, 93–105.

865 Coelho, J.P.L., Stahl, M., Bloemeke, N., Meighen-Berger, K., Alvira, C.P., Zhang, Z.-R., Sieber,
866 S.A., and Feige, M.J. (2019). A network of chaperones prevents and detects failures in
867 membrane protein lipid bilayer integration. Nat. Commun. *10*.

868 Granseth, E., von Heijne, G., and Elofsson, A. (2005). A study of the membrane-water interface
869 region of membrane proteins. J. Mol. Biol. *346*, 377–385.

870 Guna, A., Volkmar, N., Christianson, J.C., and Hegde, R.S. (2018). The ER membrane protein
871 complex is a transmembrane domain insertase. Science *359*, 470–473.

872 Ingolia, N.T., Ghaemmaghami, S., Newman, J.R.S., and Weissman, J.S. (2009). Genome-Wide
873 Analysis in Vivo of Translation with Nucleotide Resolution Using Ribosome Profiling. Science
874 *324*, 218–223.

875 Jonikas, M.C., Collins, S.R., Denic, V., Oh, E., Quan, E.M., Schmid, V., Weibezahn, J.,
876 Schwappach, B., Walter, P., Weissman, J.S., et al. (2009). Comprehensive characterization of
877 genes required for protein folding in the endoplasmic reticulum. Science *323*, 1693–1697.

878 Krishnan, M.N., Ng, A., Sukumaran, B., Gilfoy, F.D., Uchil, P.D., Sultana, H., Brass, A.L.,
879 Adametz, R., Tsui, M., Qian, F., et al. (2008). RNA interference screen for human genes
880 associated with West Nile virus infection. Nature *455*, 242–245.

881 Lee, Y.-R., Kuo, S.-H., Lin, C.-Y., Fu, P.-J., Lin, Y.-S., Yeh, T.-M., and Liu, H.-S. (2018). Dengue
882 virus-induced ER stress is required for autophagy activation, viral replication, and pathogenesis
883 both in vitro and in vivo. Sci. Rep. *8*, 489.

884 Lin, C., Amberg, S.M., Chambers, T.J., and Rice, C.M. (1993). Cleavage at a novel site in the
885 NS4A region by the yellow fever virus NS2B-3 proteinase is a prerequisite for processing at the
886 downstream 4A/4B signalase site. J. Virol. *67*, 2327–2335.

887 Lin, D.L., Inoue, T., Chen, Y.-J., Chang, A., Tsai, B., and Tai, A.W. (2019). The ER Membrane
888 Protein Complex Promotes Biogenesis of Dengue and Zika Virus Non-structural Multi-pass
889 Transmembrane Proteins to Support Infection. Cell Rep. *27*, 1666-1674.e4.

890 Ma, H., Dang, Y., Wu, Y., Jia, G., Anaya, E., Zhang, J., Abraham, S., Choi, J.-G., Shi, G., Qi, L.,
891 et al. (2015). A CRISPR-Based Screen Identifies Genes Essential for West-Nile-Virus-Induced
892 Cell Death. Cell Rep. *12*, 673–683.

893 Marceau, C.D., Puschnik, A.S., Majzoub, K., Ooi, Y.S., Brewer, S.M., Fuchs, G., Swaminathan,
894 K., Mata, M.A., Elias, J.E., Sarnow, P., et al. (2016). Genetic dissection of Flaviviridae host
895 factors through genome-scale CRISPR screens. Nature *535*, 159–163.

896 Miller, S., Sparacio, S., and Bartenschlager, R. (2006). Subcellular Localization and Membrane
897 Topology of the Dengue Virus Type 2 Non-structural Protein 4B. J. Biol. Chem. *281*, 8854–
898 8863.

899 Miller, S., Kastner, S., Krijnse-Locker, J., Bühler, S., and Bartenschlager, R. (2007). The Non-
900 structural Protein 4A of Dengue Virus Is an Integral Membrane Protein Inducing Membrane
901 Alterations in a 2K-regulated Manner. J. Biol. Chem. *282*, 8873–8882.

902 Muñoz-Jordán, J.L., Laurent-Rolle, M., Ashour, J., Martínez-Sobrido, L., Ashok, M., Lipkin, W.I.,
903 and García-Sastre, A. (2005). Inhibition of alpha/beta interferon signaling by the NS4B protein of
904 flaviviruses. J. Virol. *79*, 8004–8013.

905 Neufeldt, C.J., Cortese, M., Acosta, E.G., and Bartenschlager, R. (2018). Rewiring cellular
906 networks by members of the Flaviviridae family. Nat. Rev. Microbiol. *16*, 125–142.

907 Olzmann, J.A., Kopito, R.R., and Christianson, J.C. (2013). The Mammalian Endoplasmic
908 Reticulum-Associated Degradation System. Cold Spring Harb. Perspect. Biol. *5*.

909 Peña, J., and Harris, E. (2011). Dengue virus modulates the unfolded protein response in a
910 time-dependent manner. J. Biol. Chem. *286*, 14226–14236.

911 Płaszczyca, A., Scaturro, P., Neufeldt, C.J., Cortese, M., Cerikan, B., Ferla, S., Brancale, A.,
912 Pichlmair, A., and Bartenschlager, R. (2019). A novel interaction between dengue virus

913 nonstructural protein 1 and the NS4A-2K-4B precursor is required for viral RNA replication but
914 not for formation of the membranous replication organelle. PLOS Pathog. *15*, e1007736.

915 Puschnik, A.S., Marceau, C.D., Ooi, Y.S., Majzoub, K., Rinis, N., Contessa, J.N., and Carette,
916 J.E. (2017). A Small-Molecule Oligosaccharyltransferase Inhibitor with Pan-flaviviral Activity.
917 Cell Rep. *21*, 3032–3039.

918 Reid, D.W., Campos, R.K., Child, J.R., Zheng, T., Chan, K.W.K., Bradrick, S.S., Vasudevan,
919 S.G., Garcia-Blanco, M.A., and Nicchitta, C.V. (2018). Dengue Virus Selectively Annexes
920 Endoplasmic Reticulum-Associated Translation Machinery as a Strategy for Co-opting Host Cell
921 Protein Synthesis. J. Virol. *92*, e01766-17.

922 Roosendaal, J., Westaway, E.G., Khromykh, A., and Mackenzie, J.M. (2006). Regulated
923 cleavages at the West Nile virus NS4A-2K-NS4B junctions play a major role in rearranging
924 cytoplasmic membranes and Golgi trafficking of the NS4A protein. J. Virol. *80*, 4623–4632.

925 Savidis, G., McDougall, W.M., Meraner, P., Perreira, J.M., Portmann, J.M., Trincucci, G., John,
926 S.P., Aker, A.M., Renzette, N., Robbins, D.R., et al. (2016). Identification of Zika Virus and
927 Dengue Virus Dependency Factors using Functional Genomics. Cell Rep. *16*, 232–246.

928 Senft, D., and Ronai, Z.A. (2015). UPR, autophagy, and mitochondria crosstalk underlies the
929 ER stress response. Trends Biochem. Sci. *40*, 141–148.

930 Sessions, O.M., Barrows, N.J., Souza-Neto, J.A., Robinson, T.J., Hershey, C.L., Rodgers, M.A.,
931 Ramirez, J.L., Dimopoulos, G., Yang, P.L., Pearson, J.L., et al. (2009). Discovery of insect and
932 human dengue virus host factors. Nature *458*, 1047–1050.

933 Shao, S., and Hegde, R.S. (2011). Membrane Protein Insertion at the Endoplasmic Reticulum.
934 Annu. Rev. Cell Dev. Biol. *27*, 25–56.

935 Shurtleff, M.J., Itzhak, D.N., Hussmann, J.A., Oakdale, N.T.S., Costa, E.A., Jonikas, M.,
936 Weibezahn, J., Popova, K.D., Jan, C.H., Sinitcyn, P., et al. (2018). The ER membrane protein
937 complex interacts cotranslationally to enable biogenesis of multipass membrane proteins. ELife
938 *7*, e37018.

939 Su, H.-L., Liao, C.-L., and Lin, Y.-L. (2002). Japanese Encephalitis Virus Infection Initiates
940 Endoplasmic Reticulum Stress and an Unfolded Protein Response. J. Virol. *76*, 4162–4171.

941 Volkmar, N., Thezenas, M.-L., Louie, S.M., Juszkiewicz, S., Nomura, D.K., Hegde, R.S.,
942 Kessler, B.M., and Christianson, J.C. (2019). The ER membrane protein complex promotes
943 biogenesis of sterol-related enzymes maintaining cholesterol homeostasis. J. Cell Sci. *132*.

944 Zhang, R., Miner, J.J., Gorman, M.J., Rausch, K., Ramage, H., White, J.P., Zuiani, A., Zhang,
945 P., Fernandez, E., Zhang, Q., et al. (2016). A CRISPR screen defines a signal peptide
946 processing pathway required by flaviviruses. Nature *535*, 164–168.

947 Zou, J., Lee, L.T., Wang, Q.Y., Xie, X., Lu, S., Yau, Y.H., Yuan, Z., Geifman Shochat, S., Kang,
948 C., Lescar, J., et al. (2015). Mapping the Interactions between the NS4B and NS3 proteins of
949 dengue virus. J. Virol. *89*, 3471–3483.

950

Figure 1

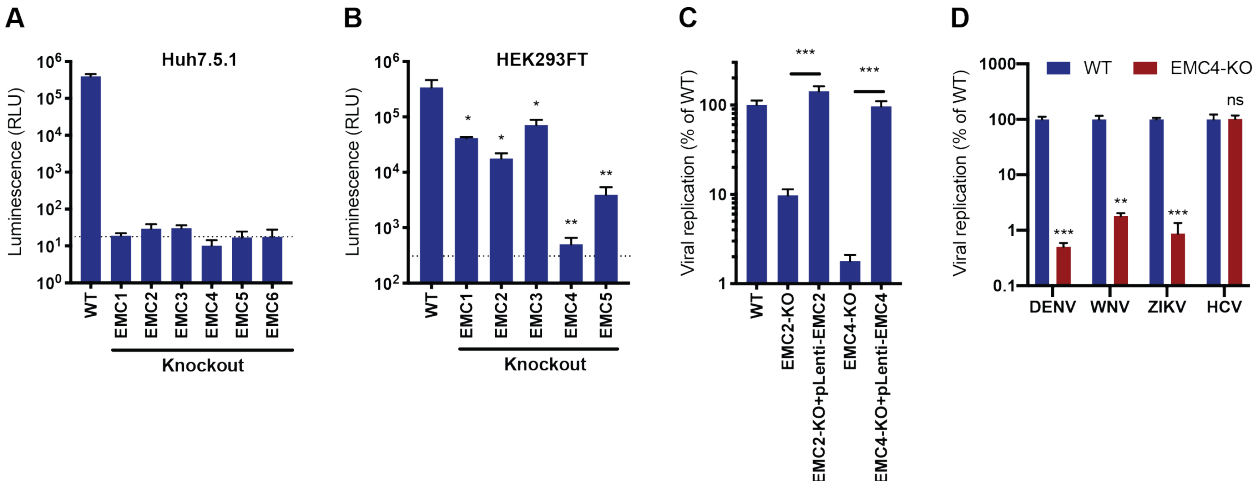
A
Huh7.5.1
Luminescence (RLU)
WT
EMC1
EMC2
EMC3
EMC4
EMC5
EMC6
Knockout
B
HEK293FT
Luminescence (RLU)
WT
EMC1
EMC2
EMC3
EMC4
EMC5
Knockout
C
Viral replication (% of WT)
WT
EMC2-KO
EMC2-KO+pLenti-EMC2
EMC4-KO
EMC4-KO+pLenti-EMC4
D
WT
EMC4-KO
Viral replication (% of WT)
ns
DENV
WNV
ZIKV
HCV

951

Figure 2

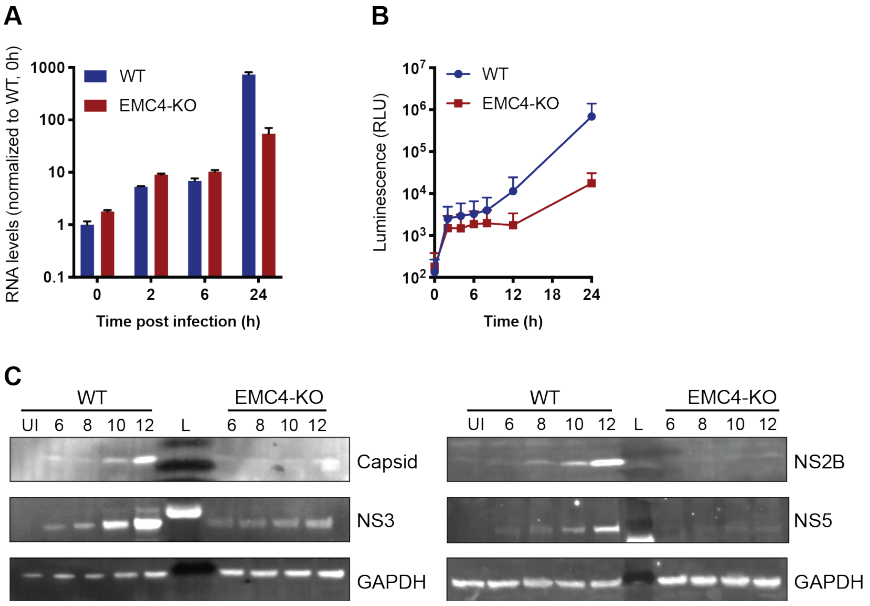
A
RNA levels (normalized to WT, 0h)
1000
100
10
1
0.1
WT
EMC4-KO
0
2
6
24
Time post infection (h)
B
Luminescence (RLU)
10^7
10^6
10^5
10^4
10^3
10^2
WT
EMC4-KO
0
6
12
18
24
Time (h)
C
WT
EMC4-KO
UI 6 8 10 12 L 6 8 10 12
Capsid
NS3
GAPDH
WT
EMC4-KO
UI 6 8 10 12 L 6 8 10 12
NS2B
NS5
GAPDH

952

Figure 3

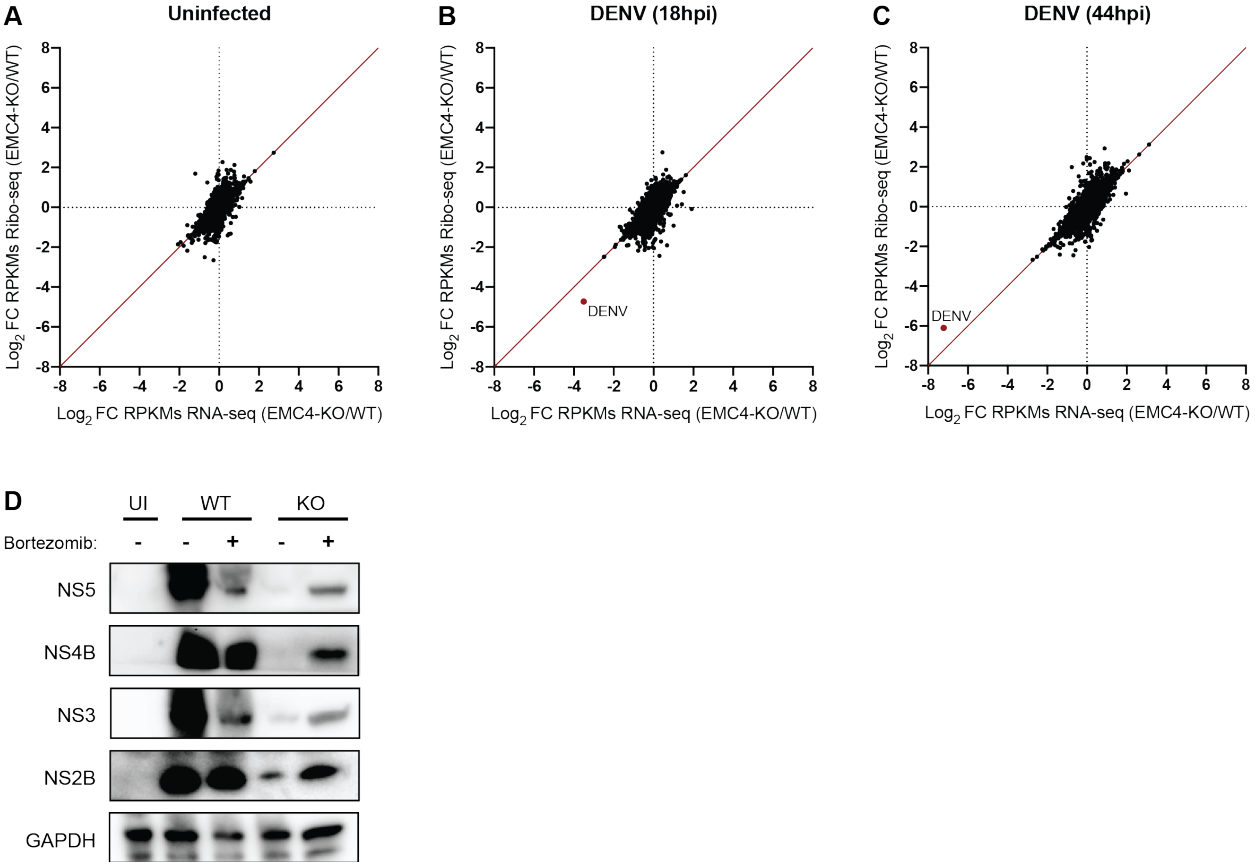
A
Uninfected
B
DENV (18hpi)
C
DENV (44hpi)
Log2 FC RPKMs Ribo-seq (EMC4-KO/WT)
Log2 FC RPKMs RNA-seq (EMC4-KO/WT)
DENV
D
UI
WT
KO
Bortezomib:
-
-
+
-
+
NS5
NS4B
NS3
NS2B
GAPDH

953

Figure 4

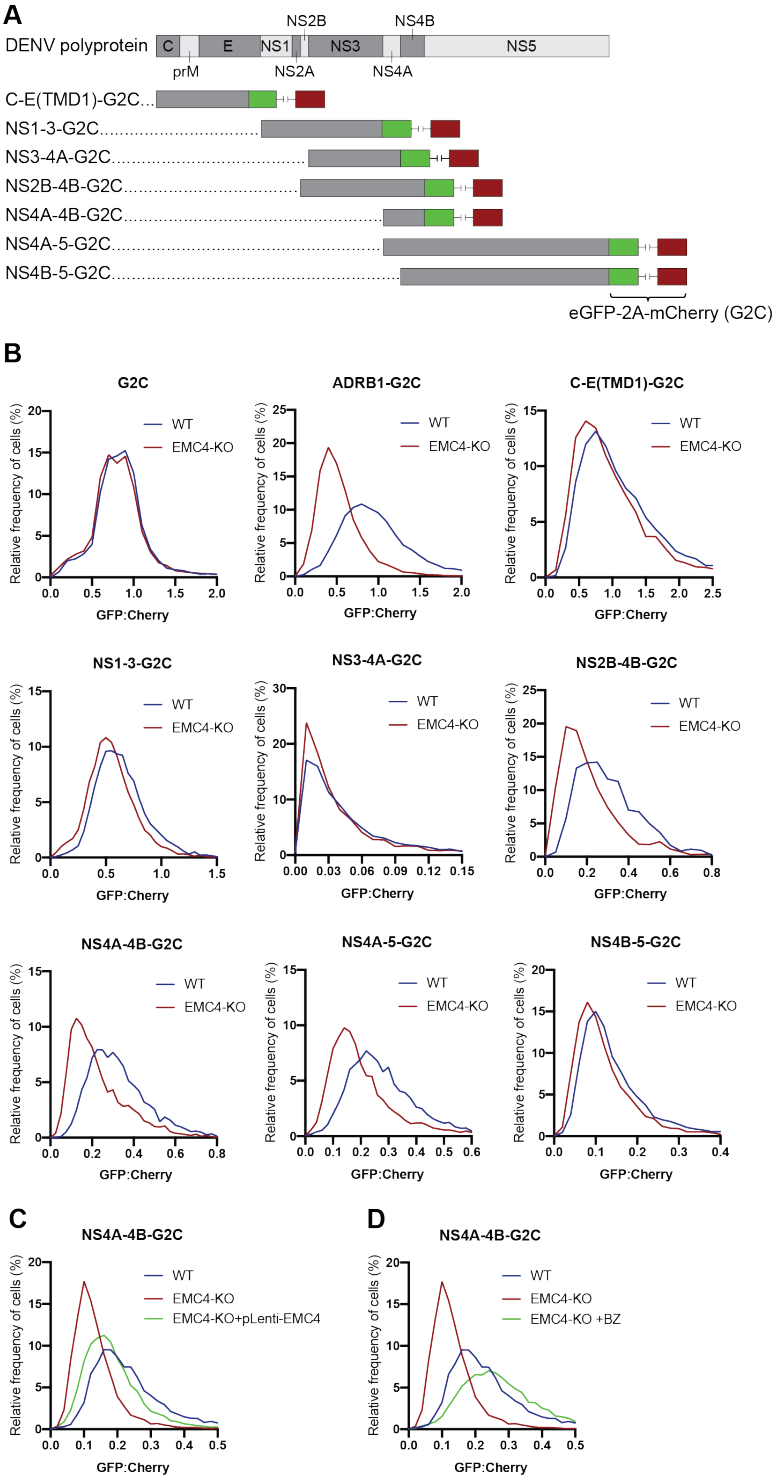
A
DENV polyprotein
C
E
NS1
NS2B
NS3
NS4B
NS5
prM
NS2A
NS4A
C-E(TMD1)-G2C...
NS1-3-G2C
NS3-4A-G2C
NS2B-4B-G2C
NS4A-4B-G2C
NS4A-5-G2C
NS4B-5-G2C
eGFP-2A-mCherry (G2C)
B
G2C
ADRB1-G2C
C-E(TMD1)-G2C
NS1-3-G2C
NS3-4A-G2C
NS2B-4B-G2C
NS4A-4B-G2C
NS4A-5-G2C
NS4B-5-G2C
WT
EMC4-KO
Relative frequency of cells (%)
GFP:Cherry
C
NS4A-4B-G2C
EMC4-KO+pLenti-EMC4
D
EMC4-KO +BZ

954

Figure 5

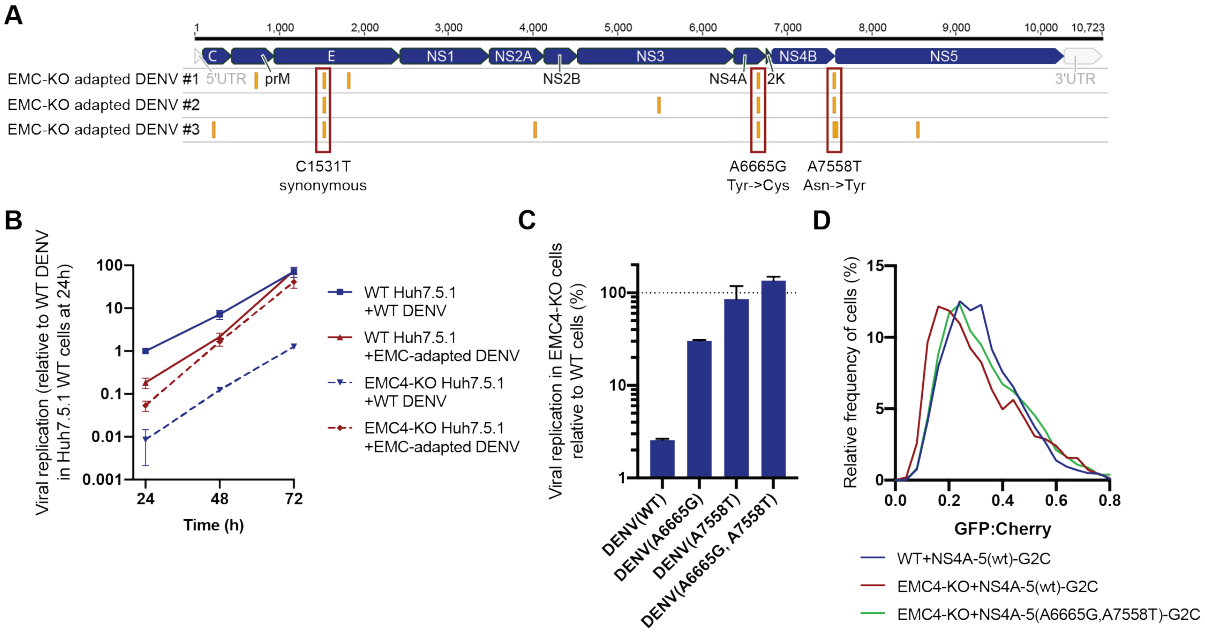
A
1
1,000
2,000
3,000
4,000
5,000
6,000
7,000
8,000
9,000
10,000
10,723
C
E
NS1
NS2A
NS3
NS4B
NS5
EMC-KO adapted DENV #1
5'UTR
prM
NS2B
NS4A
2K
3'UTR
EMC-KO adapted DENV #2
EMC-KO adapted DENV #3
C1531T
synonymous
A6665G
Tyr->Cys
A7558T
Asn->Tyr
B
Viral replication (relative to WT DENV in Huh7.5.1 WT cells at 24h)
100
10
1
0.1
0.01
0.001
24
48
72
Time (h)
WT Huh7.5.1 +WT DENV
WT Huh7.5.1 +EMC-adapted DENV
EMC4-KO Huh7.5.1 +WT DENV
EMC4-KO Huh7.5.1 +EMC-adapted DENV
C
Viral replication in EMC4-KO cells relative to WT cells (%)
100
10
1
DENV(WT)
DENV(A6665G)
DENV(A7558T)
DENV(A6665G, A7558T)
D
Relative frequency of cells (%)
15
10
5
0
0.0
0.2
0.4
0.6
0.8
GFP:Cherry
WT+NS4A-5(wt)-G2C
EMC4-KO+NS4A-5(wt)-G2C
EMC4-KO+NS4A-5(A6665G,A7558T)-G2C

955

Figure 6

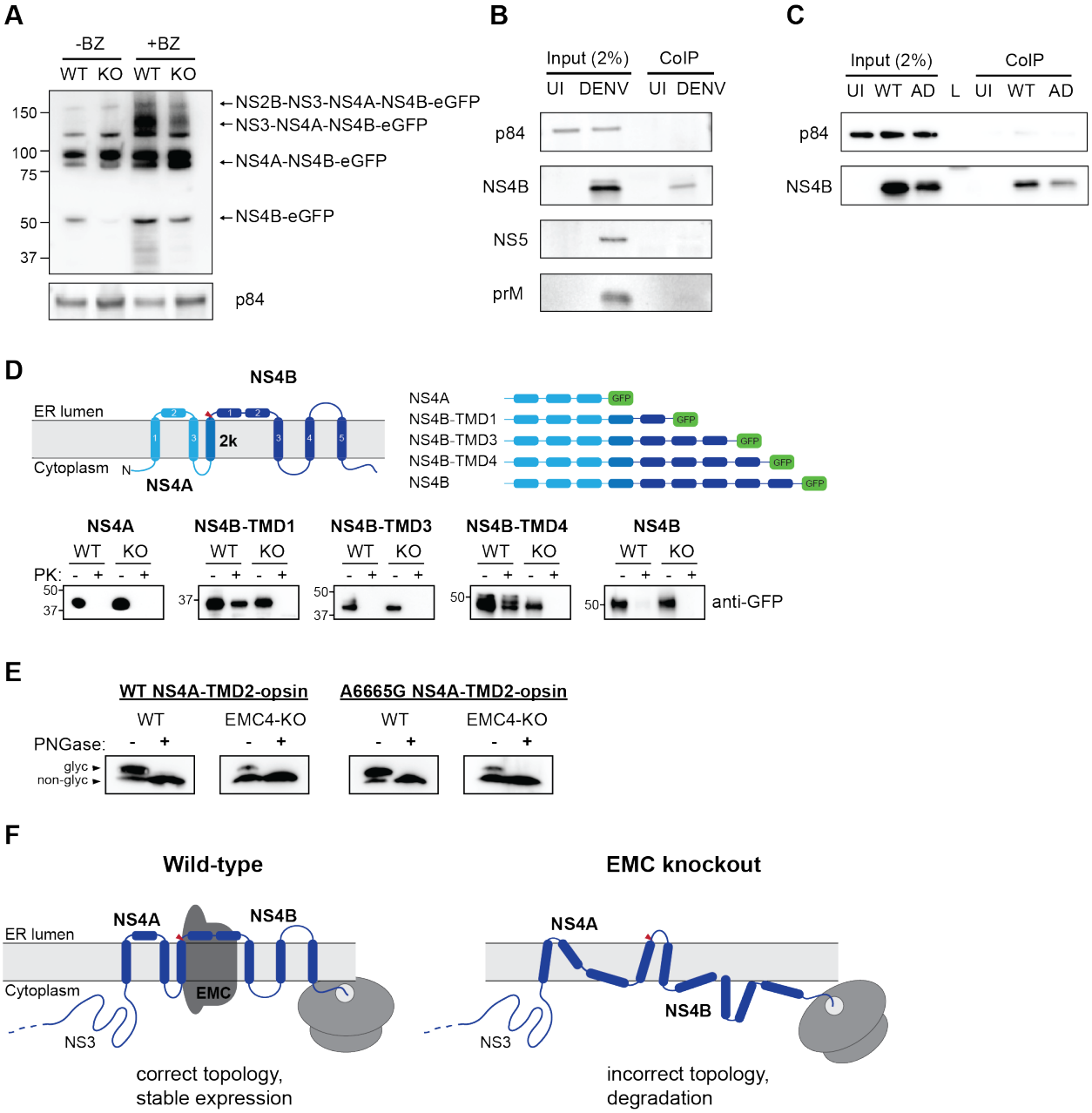
A
-BZ
+BZ
WT KO WT KO
150
100
75
50
37
NS2B-NS3-NS4A-NS4B-eGFP
NS3-NS4A-NS4B-eGFP
NS4A-NS4B-eGFP
NS4B-eGFP
p84
B
Input (2%)
CoIP
UI DENV UI DENV
p84
NS4B
NS5
prM
C
Input (2%)
CoIP
UI WT AD L UI WT AD
p84
NS4B
D
NS4B
ER lumen
Cytoplasm
N
NS4A
2k
NS4A
NS4B-TMD1
NS4B-TMD3
NS4B-TMD4
NS4B
GFP
NS4A
NS4B-TMD1
NS4B-TMD3
NS4B-TMD4
NS4B
WT KO
PK:
anti-GFP
E
WT NS4A-TMD2-opsin
A6665G NS4A-TMD2-opsin
WT
EMC4-KO
PNGase:
glyc
non-glyc
F
Wild-type
EMC knockout
ER lumen
Cytoplasm
NS4A
NS4B
EMC
NS3
correct topology,
stable expression
incorrect topology,
degradation

956

Figure 1-figure supplement 1

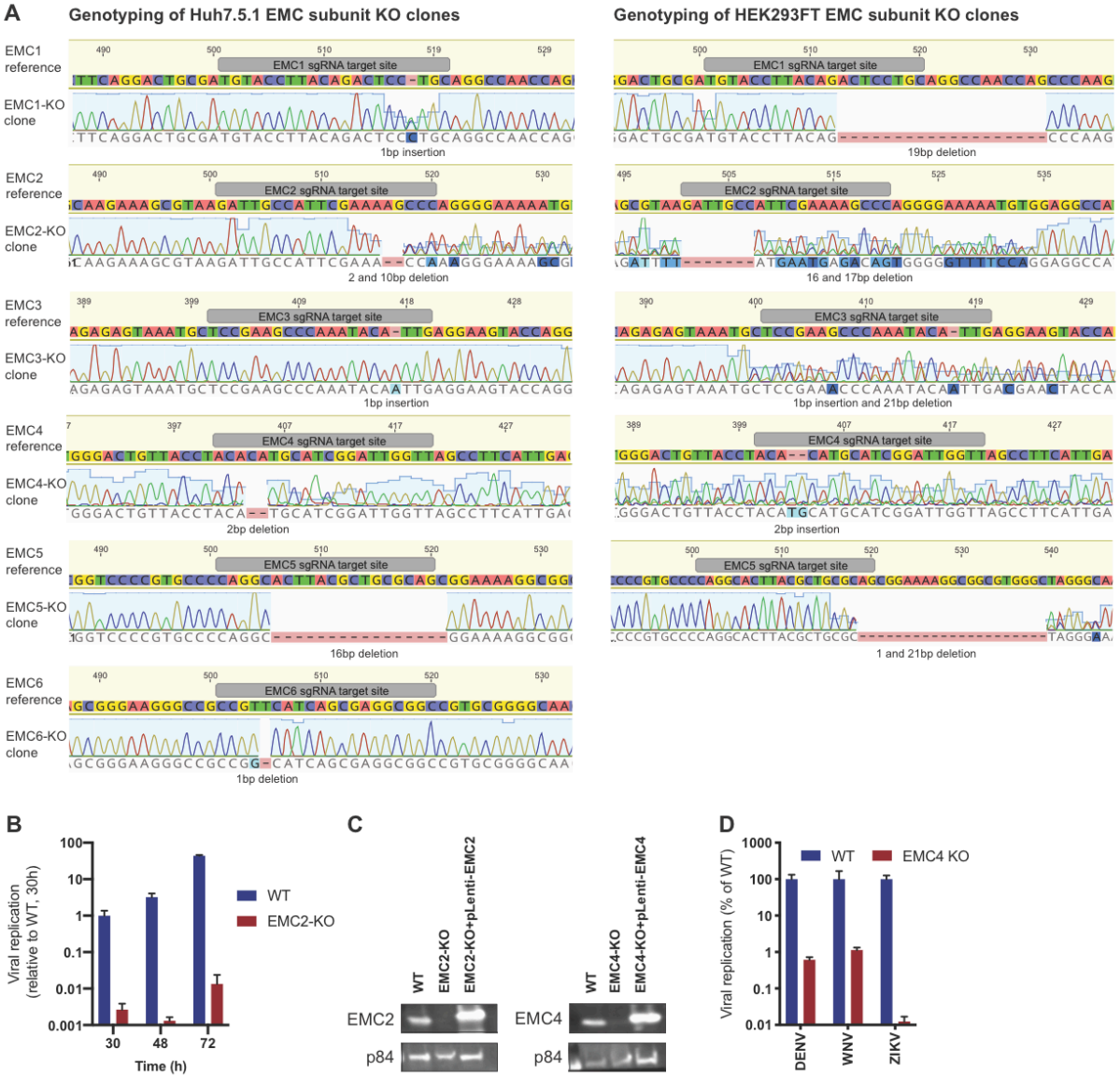

957

Figure 2-figure supplement 1

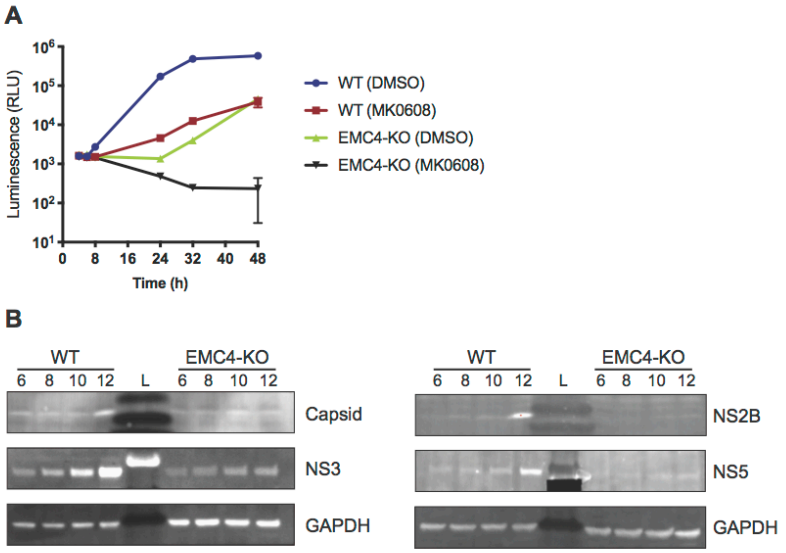

958

Figure 3-figure supplement 1

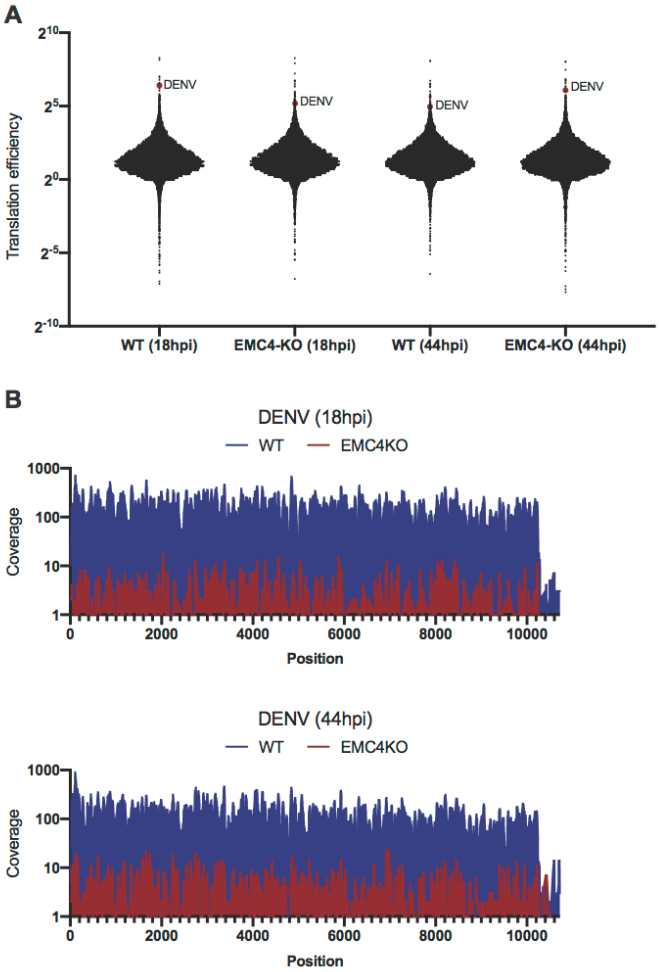

959

Figure 3-figure supplement 2

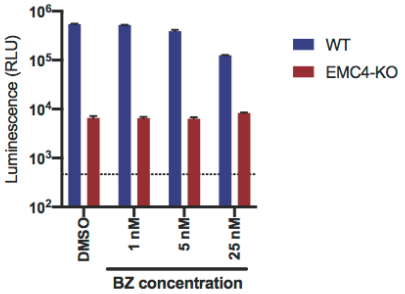

960

Figure 4-figure supplement 1

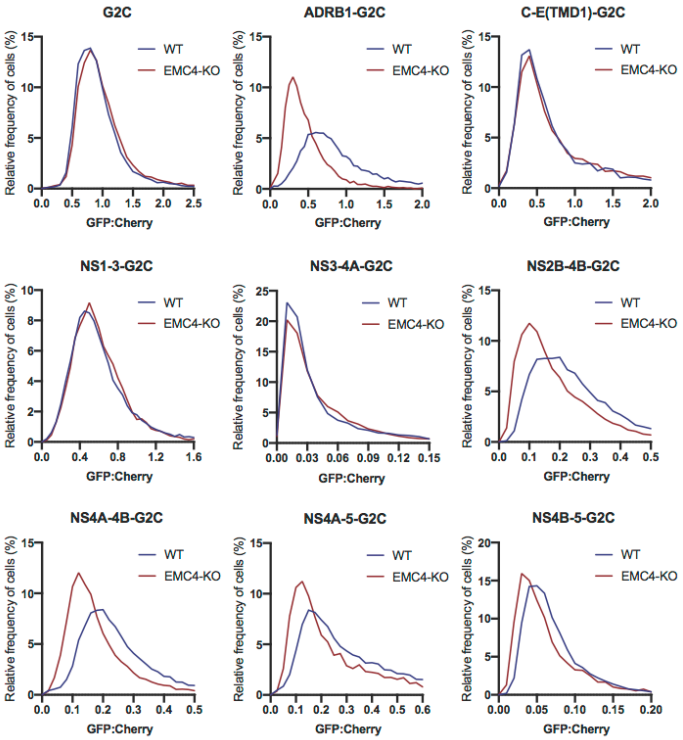

961

Figure 5-figure supplement 1

Virus isolate	Position	nt change	Coverage	Variant frequency	Reference frequency	aa change
EMC adapted DENV #3	226	T -> C	9754	99.80%	0.10%	synonymous
EMC adapted DENV #1	725	T -> C	5653	99.70%	0.10%	Val->Ala
EMC adapted DENV #1	1531	C -> T	3686	98.40%	0.80%	synonymous
EMC adapted DENV #2	1531	C -> T	9399	99.90%	0.10%	synonymous
EMC adapted DENV #3	1531	C -> T	14698	99.50%	0.20%	synonymous
EMC adapted DENV #1	1818	C -> A	3366	99.00%	0.20%	synonymous
EMC adapted DENV #3	4018	C -> T	16149	94.50%	5.50%	synonymous
EMC adapted DENV #2	5493	A -> G	10626	99.00%	0.50%	synonymous
EMC adapted DENV #1	6665	A -> G	3172	99.70%	0.10%	Tyr->Cys
EMC adapted DENV #2	6665	A -> G	8932	99.40%	0.50%	Tyr->Cys
EMC adapted DENV #3	6665	A -> G	13319	99.50%	0.20%	Tyr->Cys
EMC adapted DENV #1	7558	A -> T	4205	98.40%	0.40%	Asn->Tyr
EMC adapted DENV #2	7558	A -> T	10497	99.40%	0.10%	Asn->Tyr
EMC adapted DENV #3	7558	A -> T	16401	99.00%	0.04%	Asn->Tyr
EMC adapted DENV #3	7581	C -> T	16867	94.20%	5.70%	synonymous
EMC adapted DENV #3	8546	G -> A	15538	94.80%	5.10%	Arg->Lys

962

Figure 5-figure supplement 2

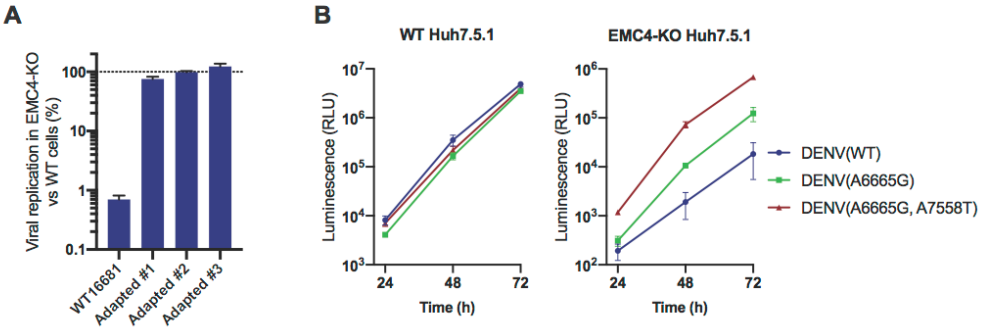

963